Journal of Molecular Liquids 330 (2021) 115605

Contents lists available at ScienceDirect

Journal of Molecular Liquids

journal homepage: www.elsevier.com/locate/molliq

Hydroxy phenyl hydrazides and their role as corrosion impeding agent: A detail experimental and theoretical study

Ashish Kumar Singh [a,*], Bhawna Chugh [b], Manjeet Singh [c], Sanjeeve Thakur [b], Balaram Pani [d], Lei Guo [e], Savas Kaya [f], Goncagul Serdaroglu [g]

[a] Department of Applied Sciences, Bharati Vidyapeeth's College of Engineering, New Delhi 110063, India
[b] Department of Chemistry, Netaji Subhas University of Technology, New Delhi 110078, India
[c] Department of Chemistry, University of Petroleum and Energy Studies, Dehradun 248007, India
[d] Department of Chemistry, Bhaskaracharya College of Applied Science, University of Delhi, New Delhi 110078, India
[e] School of Material and Chemical Engineering, Tongren University, Tongren 554300, China
[f] Sivas Cumhuriyet University, Health Services Vocational School, Department of Pharmacy, 58140 Sivas/Turkey
[g] Sivas Cumhuriyet University, Math. and Sci. Edu., 58140 Sivas, Turkey

ARTICLE INFO

Article history:
Received 15 December 2020
Received in revised form 1 February 2021
Accepted 5 February 2021
Available online 9 February 2021

Keywords:
Toxicity
Solubility
XPS
MD
EIS
Contact angle

ABSTRACT

This study presents synthesis of environmentally benign corrosion inhibitors, hydroxy acetophenone derivative namely, N′-(1-(2-hydroxyphenyl) ethylidene) acetohydrazide (ATOH), N′-(1-(2-hydroxyphenyl) ethylidene) benzohydrazide (BZOH), 2-(1-(2-hydroxyphenyl) ethylidene) hydrazine-1-carbothioamide (TSCOH) and N′-(1-(2-hydroxyphenyl) ethylidene) hydrazinecarbothiohydrazide (TCBOH) and full investigation of their protecting ability against corrosion of MS in 1 M HCl medium. A variety of electrochemical experimental techniques viz., electrochemical impedance spectroscopy, and potentiodynamic polarization coupled with different microscopic techniques viz., scanning electron microscopy, atomic force microscopy, and x-ray photoelectron spectroscopy were run to evaluate the corrosion resistive behaviour of inhibitors. The surface feature of mild steel was further analysed by measuring contact angle in different electrolytic solutions. Furthermore, these wet-chemical experimental outcomes are well complemented from results analysed from ab initio DFT study and MD simulation. Furthermore, the MD simulation outcomes helped in visualization of interaction and thereby adsorption of inhibitors on Fe (110) surface.

1. Introduction

Our current state, i.e. age of material has been evolved through periodic development and wide use of different materials such as metals/alloys, polymers (blends and composites), ceramics etc. [1]. However, the Materials Age can be regarded as successor of Stone Age.

With their progressive evolution man has learnt to use different metals and their alloys. The technical culture of humanity has been largely developed and formed because of exceptional role of metal [2]. The hardness and abundance of metals has made them as an indispensable material for the manufacturing of tools and other things. The historical names such as Bronze and Iron Age speak itself about the influence of metals on human life. Thus, metals are considered as vital for our life.

In fact the metal reserve is a measure of economy of a nation. Thus the metal can be considered as high demand natural resource for overall development of a nation. The increasing demand of metals leads peoples to go for their intensive extraction which would be resulted in to depletion of nation valuable resource.

Almost all the metals occur in the nature in the form of their ore [3]. The production or extraction of the metals involves addition of energy to their ore. Thus the extracted metals with high system's Gibbs energy are frequently susceptible to lower their system free energy due to interaction with environment [4]. So, corrosion is inevitable process that we intend to prevent but like death and taxes we must learn to deal with it. Thus, most of the metals possess a strong propensity to revert in to its most stable thermodynamic state [5]. This conversion of metals in to their native state is actually corrosion. Although, corrosion is inevitable however, different control methods can be used to lower its rate. This includes modification of metals/alloys and environment as well as both.

Modern era uses mostly alloys in place of pure metals because of their superiority over metal, as they are often harder than pure metals, more versatile for conversion in to different forms and having more corrosion resistance [6].

Iron is one of the most abundant, brittle and hard substance. However, its highly negative oxidation potential makes it susceptible to

* Corresponding author.
E-mail address: ashish.singh.rs.apc@itbhu.ac.in (A.K. Singh).

https://doi.org/10.1016/j.molliq.2021.115605
0167-7322/

corrosion. Because of much susceptibility towards corrosion, pure iron does not commonly used at commercial level. The pure iron is thus need to be alloyed with some other metal. Mild steel (MS) is primarily the most common alloy of iron possessing very less carbon content (also known as low carbon steel). High tensile strength, efficient malleability, light weight, cost effectiveness, high ductility and low brittleness make mild steel an irreplaceable material across number of industries [7]. However the low carbon content makes mild steel susceptible to corrosion.

The corrosion inhibitors have proven as one of the best corrosion combating methods compared to other methods because they make possible the use of less-expensive materials in different corrosive environments [8–11]. They offer one of the simplest solution for protection of metal in different corrosive environment. Though, there are literally number of corrosion inhibitors already studied and their selection imposes complicated problem before us. However, the toxicity and cost effectiveness of the inhibitor prompted corrosion scientists to explore the possibility of new and effective options [12–15] which can combat against the problem of metallic corrosion in different corrosive environments.

In general, presence of hetero atoms (N, S, and O) and conjugated unsaturation make the inhibitor appreciably effective for corrosion protection [16–18]. According to previous findings the ability of hetero atoms to combat corrosion follow the order as S > N > O which is related to their electronegativity and some other factors [19]. The maximum protecting ability of S atom may be due to vacant 3d-orbital which promotes retro-donation of electrons and lead to efficient chemisorption [20].

Recently, theoretical investigations have become popular these days to study the chemical reactivity of inhibitors as well as the extent of interaction with the metallic surface which is quite tedious for experimental techniques [21–24]. However, the task to develop top premium corrosion inhibitors still remain.

This paper presents the synthesis of hydroxy acetophenone derivative namely, N′-(1-(2-hydroxyphenyl) ethylidene) acetohydrazide (ATOH), N′-(1-(2-hydroxyphenyl) ethylidene) benzohydrazide (BZOH), 2-(1-(2-hydroxyphenyl) ethylidene) hydrazine-1-carbothioamide (TSCOH) and N′-(1-(2-hydroxyphenyl) ethylidene) hydrazinecarbothiohydrazide (TCBOH) and full investigation of their protecting ability against corrosion of MS in 1 M HCl medium. The experimental techniques used for the present work are electrochemical experiments, morphological tests (SEM, AFM), x-ray photoelectron spectroscopy (XPS) to investigate their protecting ability. In addition, simulation analyses were done to gather information related to the mechanism of their adsorption. Moreover, the solubility and toxicity of the inhibitors have also been accessed.

2. Experimental

2.1. Synthesis

The inhibitors were obtained by condensation of o-hydroxy acetophenone and acetyl hydrazine, benzoyl hydrazine, thiosemicarbazide and thiocarbohydrazide (1:1 ratio) in ethanol and acetic acid as a catalyst according to the scheme shown in Fig. 1. The mixture were refluxed separately for 5–6 h in a RB flask [25], the resultant solution were cooled at room temperature for 1 h. The solid obtained was filtered out, washed and recrystallized with ethanol. The recrystallized products were further used for spectral characterization.

2.2. Structural identification

The structural characterization were performed by various spectral techniques, for example, FT-IR, ^{1}H NMR, ^{13}C NMR and elemental analysis (CHN). The instruments used for these characterizations are JASCOFT/IR-5300 spectrophotometer, Jeol AL 300 FT NMR, JEOL 400 FT-NMR and CHNS analyser respectively.

2.3. Measurement of wettability of metal surface

The effect of the existence of an inhibitor on the wettability of MS surface was studied by measuring wetting angle between electrolyte solution and metal surface by sessile drop method using the instrument DSA 100.

2.4. Preparation of electrolyte and electrode

The standard electrolyte HCl solution was obtained by diluting 37% HCl supplied by Merck India. The mild steel sheet was cut in to different size ($2.5 \times 2.0 \times 0.025$ cm^3 for weight loss measurement and $7.5 \times 1.0 \times 0.025$ cm^3 with 1 cm^2 exposed area for electrochemical studies) to carry out experiments.

2.5. Electrochemical experimentation

SP-240 Biologic electrochemical workstation equipped with three-electrode cell was used to monitor the behaviour of redox reaction occurring on metallic surface in electrolytic solution. The three electrode cell contained MS strip, platinum cord and saturated calomel function as working, counter and reference electrode respectively. During electrochemical experimentation, the temperature of whole system was thermostatically kept constant at 308 K. All the electrochemical experiments were run after getting stabilised state of open circuit potential (OCP) which can be attained by keeping the electrode cell system in electrolyte solution for 30 min. Thereafter, electrochemical impedance spectroscopy (EIS) was run at open circuit potential (OCP) with frequency ranging from 10^5 to 10^{-2} Hz and alternating current (AC) having an amplitude of 20 mV.

The obtained EIS outcomes were extracted by EC lab software and analysed by the use of *Z*-fit. Using EIS data, corrosion combating ability of inhibitor can be compared with the help of Eq. (1) as [26]:

$$CCA_{\mathrm{EIS}}\% = \frac{R_{\mathrm{ct}}^{\mathrm{p}} - R_{\mathrm{ct}}^{\mathrm{a}}}{R_{\mathrm{ct}}^{\mathrm{p}}} \times 100 \tag{1}$$

where, R_{ct} signifies charge transfer resistance whereas superscripts p and a represent presence and absence of inhibitor.

The EIS experiments were followed by potentiodynamic polarization with potential sweep ±250 mV and 1 mV/s scan rate. The performance of inhibitors can be compared on the basis of polarization data as [27]:

$$CCA_{\mathrm{PDP}}\% = \frac{i_{\mathrm{corr}}^{\mathrm{a}} - i_{\mathrm{corr}}^{\mathrm{p}}}{i_{\mathrm{corr}}^{\mathrm{a}}} \times 100 \tag{2}$$

where, i_{corr} described corrosion current density while the superscripts 'a' and 'p' described the absence and presence of inhibitor.

2.6. Weight loss investigation

MS of composition listed in Table 1 were used to prepare $2.5 \times 2 \times 0.025$ cm^3 sized coupons. These coupons were successively abraded with different grade emery paper to get desired MS surface to run weight loss experiments. From the initial and ending weight of MS coupons, inhibitor's performance can be assessed as [28]:

$$CCA_{\mathrm{WL}}\% = \frac{w^{\mathrm{a}} - w^{\mathrm{i}}}{w^{\mathrm{a}}} \times 100 \tag{3}$$

where, *w*, superscripts a, and i are written for weight loss, absence and presence of inhibitor respectively.

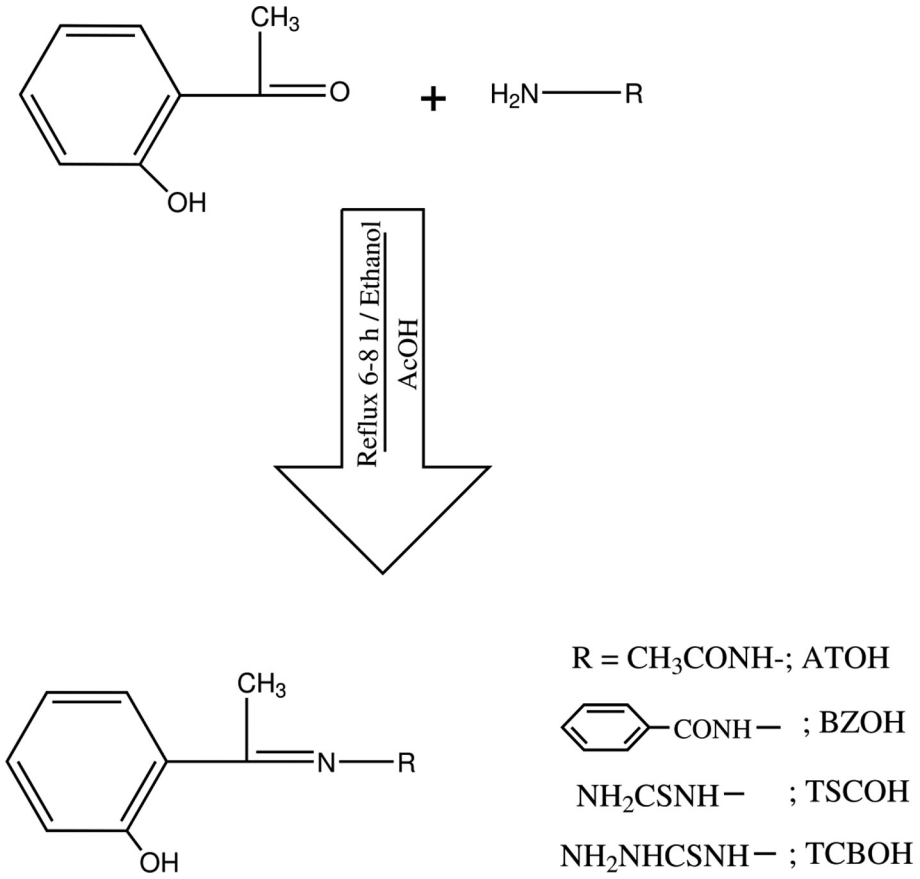

Fig. 1. Synthetic route of different inhibitors, ATOH, BZOH, TSCOH, and TCBOH.

Table 1
% composition of mild steel used in the study.

Elements	W%
C	0.05
Si	0.09
Mn	0.20
S	0.01
P	0.012
Ni	0.0025
Cr	0.001
Fe	Remaining

2.7. Topographical study of MS surface

2.7.1. SEM & AFM

The effect of electrolyte solution on the topography of electrode surface was analysed by SEM and AFM. The mild steel strips of defined size were hanged in tested solutions which may or may not have inhibitor for 6 h. After the experiment, the samples were taken out, cleaned and used to scan through SEM (Hitachi TM 3000) and AFM (Model Bruker). The AFM images were further examined by using a software Nanoscope 8.5.

2.8. XPS

The nature and basic composition of inhibitor's film adsorbed on metallic surface can be effectively examined by XPS. The X-ray photoelectron spectra were scanned by Multiprobe Surface Analysis instrument provided by Scienta Omicron, Germany. All the peaks were analysed by CASA software.

2.9. Theoretical assessment

2.9.1. Toxicity & solubility analysis

The toxicity and solubility of the researched inhibitors were evaluated. The toxic parameters were computed by the TOPKAT module of Discovery Studio software, which is focussed on the quantitative structure-activity relationship (QSAR) model, a mathematical formulation employed to explain toxicity in relevance to the physical properties of the chemical structure. While the aqueous solubilities were assessed by the Advanced Chemistry Development (ACD/Labs 6.0) software.

2.9.2. Quantum chemical calculations

All B3LYP [29,30] computations for ATOH, BZOH, TSCOH and TCBOH compounds were performed at 6-31 g(d,p), 6–311 + g(d,p) and 6–311 ++g(2df,2pd) basis sets by G09W [31] package. SMD [32] solvation model was used to conduct the water phase calculations. After geometry optimizations and verifying these structures, the NBO (natural Bond Orbital) computations [33,34] were employed at B3LYP/6–311++G(2df,2pd) level to analyse the intra-molecular interactions. Addition, the DFT- based reactivity identifiers [35–37] were calculated in the gas as well as water phases. Also, the nucleophilic and electrophilic attack sites for each compound were demonstrated by HOMO, LUMO and MEP plots. The optimized geometries and atom labelings of four compounds were given in Fig. 2.

Conceptual Density Functional Theory [38] called as DFT of chemical reactivity provides great facilities to scientists in view of the practical interpretation of chemical reactivity descriptors such as chemical potential, electronegativity, hardness and softness. In this theory, the relation of the total electronic energy and the number of electrons at a constant external potential aforementioned quantum chemical descriptors are illustrated via the subsequent equations. The equations in

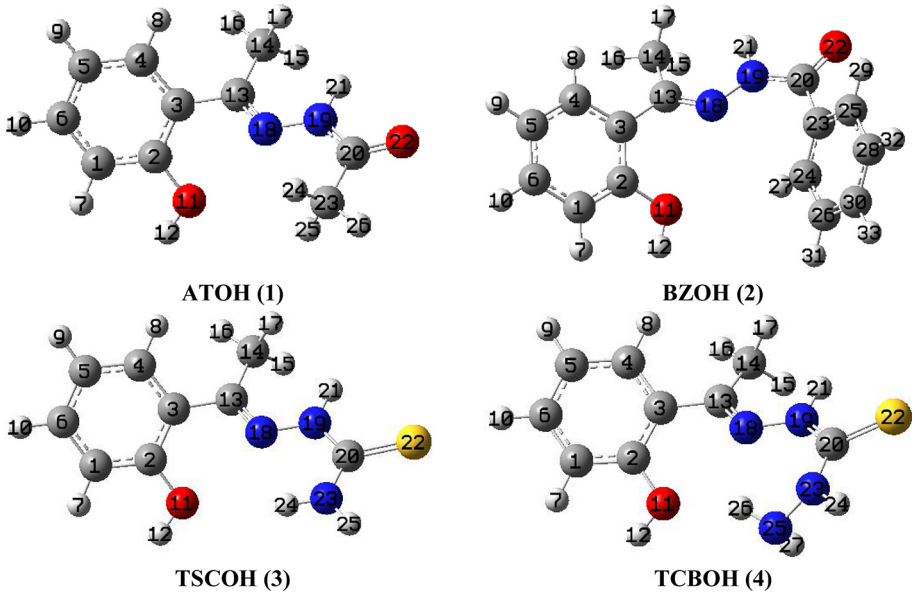

Fig. 2. The optimized structures of four compounds at B3LYP/6–311++G(2df,2pd) level in the water phase.

accordance with ionization energy and electron affinity parameters of the descriptors have been obtained by Pearson and Parr using finite differences approach [39].

$$\mu = -\chi = \left[\frac{\partial E}{\partial N}\right]_{v(r)} = -\left(\frac{I+A}{2}\right) \tag{3}$$

$$\eta = \frac{1}{2}\left[\frac{\partial^2 E}{\partial N^2}\right]_{v(r)} = \frac{I-A}{2} \tag{4}$$

$$\sigma = 1/\eta \tag{5}$$

Within the framework of Koopmans Theorem [35], ionization energy and electron affinity parameters are associated with frontier orbital energies. This theory illustrates that the negative values of HOMO and LUMO orbital energies of any compound is related to the ionization energy and electron affinity values of a compound. The relation could be written in the form of following equations:

$$I = -E_{HOMO} \tag{6}$$

$$A = -E_{LUMO} \tag{7}$$

Parr, Szentpaly and Liu modelled electrophilicity index [36] used to describe their electrophilic power on the basis of the electronegativity and chemical hardness values of chemical moeities via the subsequent expression. Then Chattaraj [40] presented the nucleophilicity in terms of the multiplicative inverse of electrophilicity index. Following these studies, in recent years, Gazquez [41] and co-workers proposed some expressions to predict electron donating and electron accepting powers of the compounds. To calculate the Gazquez parameters, we need only ionization energy and electron affinity values of the substances.

$$\omega = \chi^2/2\eta \tag{8}$$

$$\varepsilon = 1/\omega \tag{9}$$

$$\omega^+ = (I+3A)^2/(16(I-A)) \tag{10}$$

$$\omega^- = (3I+A)^2/(16(I-A)) \tag{11}$$

Polarizability (α) that is one of the useful reactivity descriptors is calculated depending on diagonal components of polarizability tensor.

$$\langle\alpha\rangle = 1/3\left[\alpha_{xx} + \alpha_{yy} + \alpha_{zz}\right] \tag{12}$$

2.9.3. MD simulations analysis

The MD simulation was carried out employing the Forcite module of Materials Studio 8.0 software developed by BIOVIA Inc. It was performed in a simulation box (1.73 nm × 1.73 nm × 3.51 nm) with periodic boundary conditions. The box comprises of a lower Fe slab and an upper solvent layer (having 400 water molecules and 1 inhibitor molecule of interest). For an iron substrate, Fe (110) was chosen as studied surface as it has a density packed structure and is highly stable, which was formulated with a six-layer Fe slab. In such model, there were 49 Fe atoms in every layer symbolising a (7 × 7) unit cell. The whole system was conducted at 298 K regulated by the Andersen thermostat, NVT canonical ensemble, with a time step of 1.0 fs and simulation time of 1000 ps, using the COMPASSII force field. Electrostatic interactions were computed using Ewald summation technique and atom based summation approach for Van der Waals interaction.

3. Result and discussion

3.1. Synthesis protocol

The synthesis of inhibitors was confirmed using spectral characterization and elemental composition (CHN analysis). The data of FT-IR, ^{1}H NMR, ^{13}C NMR and CHN analysis are presented in Table 2.

3.2. Analysis of wettability of metal surface

The contact angle measurement provided an all-important information about the wettability of metal surface to the electrolytic solution in presence of varying amount of studied compounds in electrolytic solution. The least contact angle of metal surface to the bare electrolytic solution (Fig. 3) confirmed its most hydrophilic behaviour for metal surface. Addition of different amounts of studied inhibitors increased the contact angle and thereby lessened the wettability of metal surface

Table 2
Synthesis characterization data of inhibitors.

Inhibitors	M. P. (° C)	CHN (%)	FT-IR (ν cm^{-1})	^{1}H NMR (δ ppm)	^{13}C NMR (δ ppm)
ATOH	167	C = 62.5, H = 6.3, N = 14.55	1665 (C=N), 3445 (OH; phenolic), 1680 (C=O), 3360 (-NH), 2880 (CH_3), 3078 (ArH)	6.8–7.3 (4H; m, Phenyl); 13.1 (1H; s, OH); 1.6 (3H; s, CH_3); 10.3 (1H; s, NH); 1.9 (3H; s, CH_3-Acetyl group)	116.7, 118.0, 121.1, 130.8, 132.0 (aromatic); 161.8 (aromatic C-OH); 166.8 (C=N); 172.1 (CONH); 18.2 (CH_3 attached to C=N) and 20.5 (CH_3 –acetyl group)
BZOH	172	C = 75.2, H = 5.5, N = 5.8	1660 (C=N), 3440 (OH; phenolic), 1640 (C=O), 3350 (-NH), 2854 (CH_3), 3072 (ArH)	6.8–7.32 (4H; m, Phenyl); 13.2 (1H; s, OH); 1.75 (3H; s, CH_3); 10.7 (1H; s, NH); 7.5–7.9 (5H; m,)	117.8, 118.5. 121.2, 127.5. 128.2, 132.1, 132.4 (aromatic); 162.5 (aromatic C-OH); 167.2 (C=N); 17.8 (CH_3 attached to C=N) and 162.8 (CONH)
TSCOH	206	C = 51.6, H = 5.3, N = 20.10	1610 (C=N), 3450 (Phenolic OH), 3371 (NH_2), 3240 (NH), 2877 (CH_3), 3066 (ArH), 1260 (C=S), 708 (CS)	6.81–7.32 (4H; m, Phenyl); 13.15 (1H; s, OH); 1.8 (3H; s, CH_3); 11.3 (1H; s, NH); 7.68 (1H, s, $CSNH_2$)	116.3, 118.2, 121.0, 132.0, 132.4 (aromatic); 163.4 (aromatic C-OH); 168.1 (C=N); 16.8 (CH_3 attached to C=N); 180.2 (C=S)
TCBOH	195	C = 48.3, H = 5.4, N = 24.99	1655 (C=N), 1245 (C=S), 710 (CS), 2975 (CH_3), 3485 (OH), 3005 (ArH)	6.75–7.32 (4H; m, Phenyl); 13.2 (1H; s, OH); 1.85 (3H; s, CH_3); 10.5 (1H, s, =N-NH); 8.52 (1H, t, NH-NH_2); 4.3 (2H, d, NH_2)	117.2, 118.5, 121.4, 132.0, 132.6 (aromatic); 163.8 (aromatic C-OH); 167.0 (C=N); 17.6 (CH_3 attached to C=N); 182.8 (C=S)

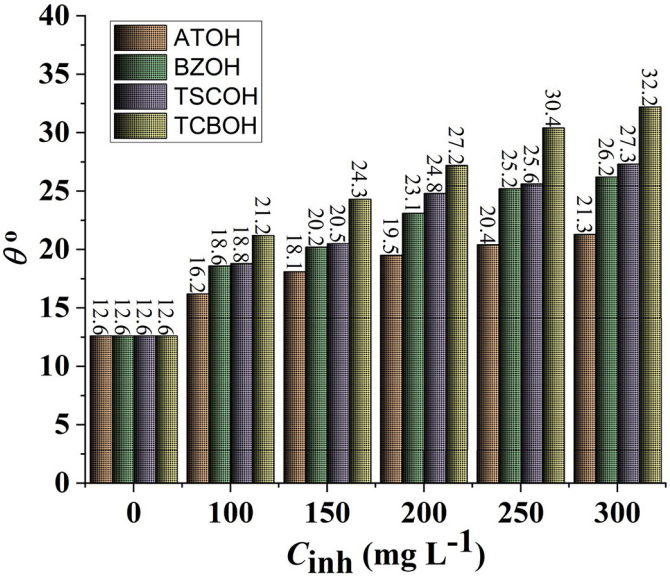

Fig. 3. Variation of contact angle of MS surface to the different electrolytic solutions.

for electrolytic solution. The order of wettability of metal surface for different inhibitor solution is ATOH < BZOH < TSCOH < TCBOH. This order confirmed their corrosion combating ability.

3.3. Electrochemical experiment analysis

3.3.1. Open circuit potential

The thermodynamic ability of a substance to be oxidized electrochemically could be assessed by measuring its OCP. The change of OCP by the presence of inhibitors relative to that in blank acid is appreciably supportive to interpret which electrochemical process whether cathodic or anodic is largely controlled by the presence of various amount of inhibitors [42]. The open circuit potential of MS immersed in different inhibitor's solution is presented as Fig. 4. The presence of all the inhibitors moved the OCP chiefly in negative direction which confirmed the inhibitor's influence over cathodic reaction under the experimental condition.

3.3.2. Electrochemical impedance spectroscopy (EIS)

Potentiostatic EIS studies were run for MS working electrode immersed in various solutions. The results of the experiment are presented as Nyquist and Bode-Phase angle curves (Fig. 5). Table 3 contained all the EIS results achieved through fitting of the experimental data using relevant equivalent circuit. The shape of Nyquist plots obtained after running EIS experiments on MS dipped in different solutions reflected that the impeding behaviour of the inhibitors ATOH, BZOH, TSCOH and TCBOH was determined collectively by resistance, capacitance and inductance. Though their impeding behaviour were controlled by resistance, capacitance and inductance, but, since dominant part of Nyquist plots occurred in +Y-direction which inferred the major role of resistance and capacitance in controlling the impedance behaviour of these inhibitors, ATOH, BZOH, TSCOH and, TCBOH.

The Nyquist curves attained in this experiment showed two loops; one capacitive at higher frequency associated with a low-frequency inductive loop. There may be two reasons behind the formation of inductive loop; first one the strong adsorption of inhibitors or second one, the relaxation phenomena's caused by adsorption of Cl^{-}_{ads}, and H^{+}_{ads} [43]. However, a large size of inductive loop with increasing concentration of inhibitors confirmed that it is the strong adsorption of inhibitor which is responsible for the formation of inductive loop [44].

The inhomogeneity or surface roughness of solid electrode resulted in to depressed semi-circled Nyquist plots which would be perfect semicircle otherwise [45]. This results in to substitution of double layer capacitance (C_{dl}) by constant phase element (*CPE*) to get an appropriate equivalent circuit (Fig. 6a) which can be more accurately fitted with the experimental results. The fitting of experimental data with given equivalent circuit is represented in Fig. 6b-c (EIS data attained with 300 mg L^{-1} TCBOH).

Using Eq. (13), the impedance can be obtained as

$$Z_{CPE} = R_s + \left[1/\left\{(j\omega)^{n}Q + 1/(R_{ct} + 1/(j\omega L + 1/R_L)))\right\}\right] \quad (13)$$

where, Z_{CPE}, j, ω and n signify magnitude of *CPE*, an imaginary number ($j^2 = -1$), angular frequency and degree of inhomogeneity.

Angular frequency (ω) and double layer capacitance C_{dl} can be obtained as [46]:

$$\omega = (QR_{ct})^{-n} \quad (14)$$

$$C_{dl} = \left(QR_{ct}^{1-n}\right)^{1/n} \quad (15)$$

The value of n ranges within 0 and 1; It explains the deviation from an ideal behaviour.

The C_{dl} and thickness of protective film are related to each other as per Gibb's Helmholtz model presented as [47]:

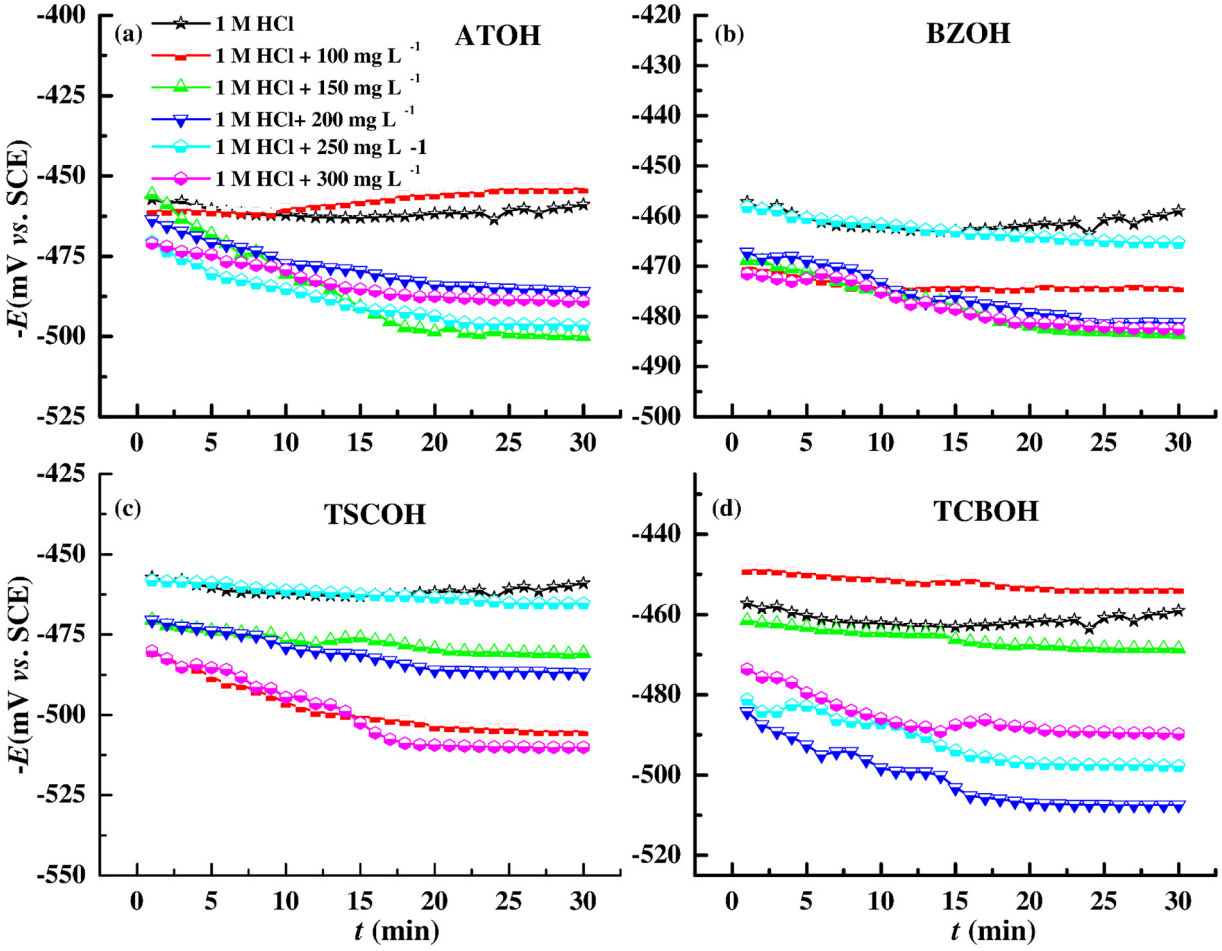

Fig. 4. Variation of OCP against concentration of (a) ATOH, (b) BZOH, (c) TSCOH, and (d) TCBOH.

$$C_{dl} = \frac{\varepsilon\varepsilon_0 A}{d} \tag{16}$$

where, ε, ε_0, A and d, are dielectric constant, vacuum permittivity, area of electrode and thickness of electric double layer. The calculated C_{dl} data are presented in Table 3.

A close overview of all the data attained from EIS (shown in Table 3) makes it known that the increasing inhibitor's concentration increases R_{ct} on one side and reduces C_{dl} on the other. This displays the deposit of protective layer that slows down the process of charge transfer.

An observation of Bode plots obtained with different inhibitor's amount confirms the presence of single time constant during the process occurring on the electrode surface. Demonstration of phase angle plots showed that the phase angle shifted towards more negative value with increasing inhibitor's amount. It confirms the increasing capacitive behaviour of inhibitors at their higher concentrations [48].

3.3.3. Tafel polarization

Polarization study offers primarily the best method to investigate corrosion of metals and their protecting abilities. The extrapolation of polarization plots has made possible the computation of different polarization parameters [49] listed in Table 4.

The potentiodynamic polarization plots of MS obtained in different electrolytic solutions are presented as Fig. 7a-d. An overview of polarization curves demonstrates clearly that polarization curves obtained for different inhibitors, ATOH, BZOH, TSCOH, and TCBOH are very much similar. This is an indication of similar mechanism of inhibition taking place at electrode surface after adsorption of different inhibitors.

Fig. 7a-d shows that both anodic and cathodic processes are inhibited significantly for electrolytic solution having inhibitors. However, this suppression is more noticeable in case of cathodic reactions which is further supported by a more pronounced change of cathodic Tafel slope (b_c) compared to anodic Tafel slope (b_a) [50].

The shift in the value of E_{corr} related to blank solution decides the nature of inhibitor. An E_{corr} shift >85 mV confirms a cathodic/anodic nature of an inhibitor whereas <85 mV corresponds to mixed nature behaviour of inhibitor [51]. In this investigation, E_{corr} shift was found <85 mV that affirmed the mixed type behaviour of inhibitors, ATOH, BZOH, TSCOH, and TCBOH.

The relation between corrosion current density and corrosion rate is written as [43]:

$$3.27 i_{corr}\left(\frac{\text{Eq.wt.}}{\text{d}}\right) = C_R \tag{17}$$

where all the symbols have their usual meaning.

The value of C_R obtained from above relationship are listed in Table 4 along with other polarization parameters. The obtained C_R value follow the same trend as calculated from other methods.

The best performance of TCBOH compared to other inhibitors is related to presence of electron-rich hetero atoms which facilitates its adsorption over the electrode surface and thereby reduces corrosion rate up to maximum extent.

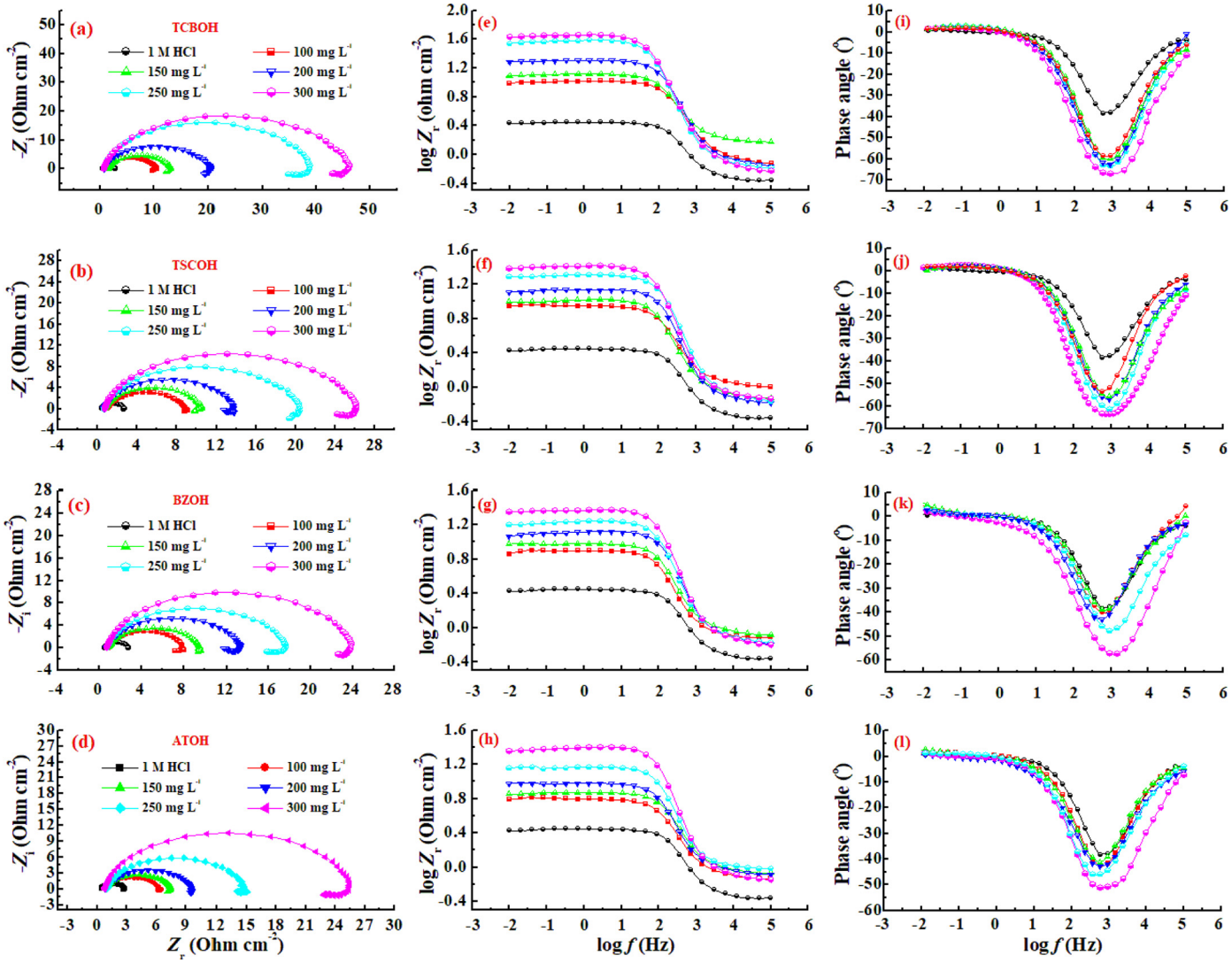

Fig. 5. Nyquist plots of MS in acid solution in absence and presence of (a) ATOH, (b) BZOH, (c) TSCOH, and (d) TCBOH; Bode plots (e) ATOH, (f) BZOH, (g) TSCOH, and (h) TCBOH; Phase angle plots (i) ATOH, (j) BZOH, (k) TSCOH, and (l) TCBOH.

Table 3
EIS parameters obtained for mild steel in HCl solution in absence and presence of inhibitors.

Name of Inhibitor	Conc. of Inhibitor (mg L^{-1})	R_s (Ω cm^2)	R_{ct} (Ω cm^2)	R_L (Ω cm^2)	L (H)	Q ($\mu F.s^{(n-1)}$)	n	C_{dl} (μF cm^{-2})	CCA_{EIS}%
1M HCl	–	0.43	3.26	0.80	10.3	719.2	0.801	157.1	–
ATOH	100	0.85	6.10	1.10	10.0	490.1	0.813	128.7	46.55
	150	0.86	7.11	1.70	9.00	430.2	0.822	122.8	54.14
	200	0.92	9.40	2.60	7.80	360.0	0.831	113.2	65.31
	250	1.60	14.36	4.30	7.10	310.3	0.832	104.0	77.29
	300	0.94	22.61	5.90	6.50	266.2	0.835	98.2	85.58
BZOH	100	0.80	7.20	1.70	9.80	462.2	0.815	126.6	54.72
	150	1.62	9.40	1.50	8.70	391.3	0.824	118.3	65.31
	200	0.90	11.76	3.60	7.50	313.6	0.833	101.9	72.27
	250	1.20	15.80	4.80	7.00	280.2	0.836	96.7	79.36
	300	0.95	22.86	5.80	6.20	242.3	0.839	89.4	85.73
TSCOH	100	1.40	8.83	1.20	8.30	412.3	0.820	120.2	63.08
	150	1.22	9.86	2.60	7.90	356.5	0.828	110.2	66.93
	200	0.92	12.74	3.90	6.90	273.1	0.835	89.2	74.41
	250	1.10	19.33	4.90	6.00	236.5	0.840	84.8	83.13
	300	1.12	24.20	6.10	5.50	196.4	0.844	73.1	86.52
TCBOH	100	0.82	9.10	1.60	7.10	368.2	0.824	109.1	63.77
	150	1.65	12.10	2.20	6.30	305.1	0.831	97.7	73.05
	200	1.10	18.80	2.80	5.90	240.1	0.841	86.5	82.65
	250	1.00	34.79	5.60	5.30	174.2	0.850	70.8	90.62
	300	0.95	43.00	6.10	4.80	120.8	0.856	49.8	92.41

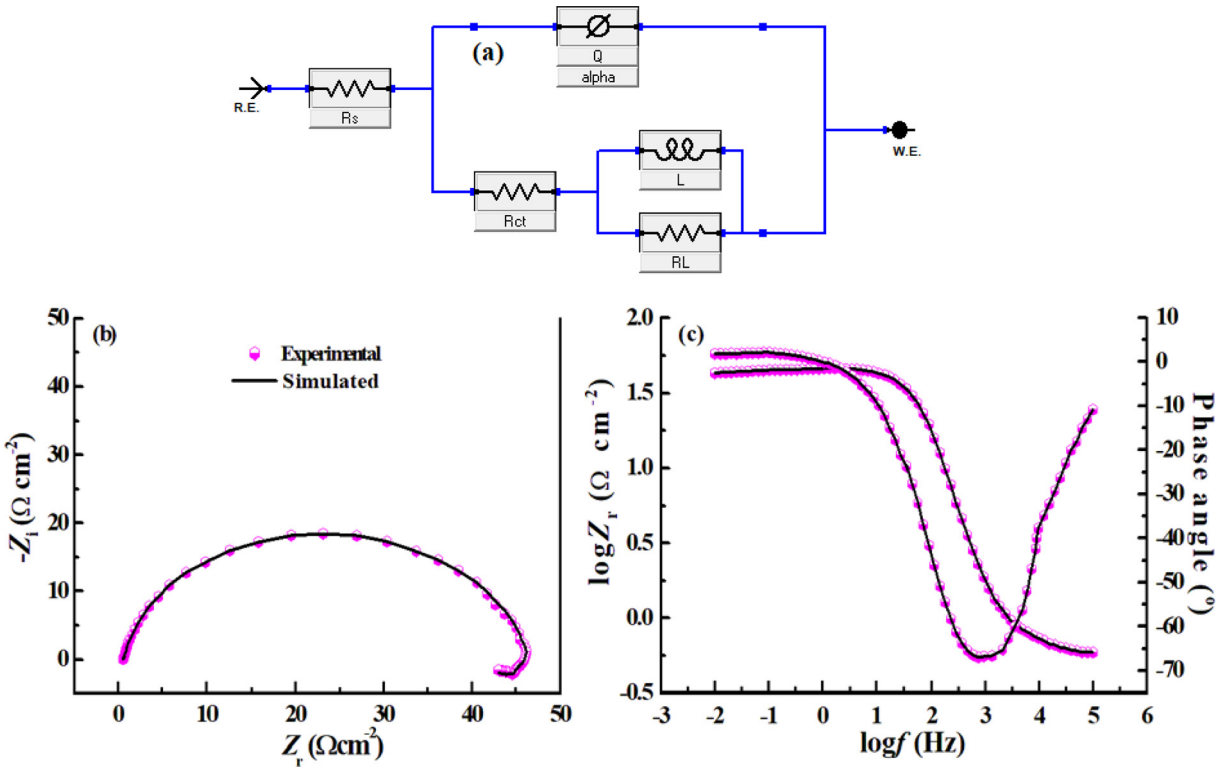

Fig. 6. (a) proposed equivalent electrochemical circuit (b) and (c) Fitting of experimental data with proposed equivalent circuit obtained with 300 mg L^{-1} of TCBOH.

3.4. Weight loss investigation

3.4.1. Corrosion rate vs. inhibitor's amount

Gravimetric analysis is one of the most common method used to find out the role of inhibitor's amount on corrosion rate of metals when exposed to aggressive corrosive solution. The results obtained from weight loss investigation is shown as Fig. 8a which shows a steady decrease in the weight loss with increasing inhibitor's concentration. Among all the studied inhibitors, TCBOH shown excellent performance which is because of the existence of electron rich hetero atoms which ease its adsorption on MS surface to lessen the corrosion rate.

3.4.2. Effect of inhibitor on corrosion kinetics

The role of inhibitor's presence on the corrosion kinetics can be established by carrying out gravimetric analyses at different temperatures ranging from 308 to 338 K with a difference of 10 K.

Applying Arrhenius and Eyring transition state equations on corrosion kinetics, different kinetic parameters were found as [52,53]:

$$\log C_R = \frac{-E_a}{2.303RT} + \log \lambda \quad (18)$$

Table 4
Polarization parameters obtained for mild steel in HCl solution in absence and presence of inhibitors.

Electrolyte solution	Inhibitor	Concentration (mg L^{-1})	$-E_{corr}$ (mV vs. SCE)	i_{corr} (μA cm^{-2})	β_a (mV dec^{-1})	β_c (mV dec^{-1})	C_R (mmy^{-1})	CCA_{PDP}%
1M HCl	–	–	459	2600	119.2	190.7	30.6	–
	ATOH	100	454	1390	126.8	146.4	16.3	46.5
		150	500	1192	103.0	240.0	14.0	54.1
		200	486	902	136.4	251.2	10.6	65.3
		250	500	590	107.0	154.8	6.9	77.3
		300	492	375	133.1	164.6	4.4	85.5
	BZOH	100	475	1177	98.6	142.4	13.8	54.7
		150	484	902	130.4	254.2	10.6	65.3
		200	481	721	98.7	119.8	8.5	72.3
		250	466	536	107.3	252.2	6.30	79.4
		300	486	371	97.0	222.6	4.3	85.7
	TSCOH	100	506	960	92.3	168.9	11.3	63.1
		150	479	860	98.8	189.2	10.1	66.9
		200	487	665	97.0	154.8	7.8	74.4
		250	467	438	80.7	185.0	5.1	83.1
		300	512	350	85.8	117.1	4.1	86.5
	TCBOH	100	452	942	94.8	130.7	11.1	63.8
		150	470	700	100.9	248.2	8.2	73.1
		200	513	451	132.6	278.7	5.3	82.6
		250	500	243	101.2	130.8	2.8	90.6
		300	491	197	93.3	121.4	2.3	92.4

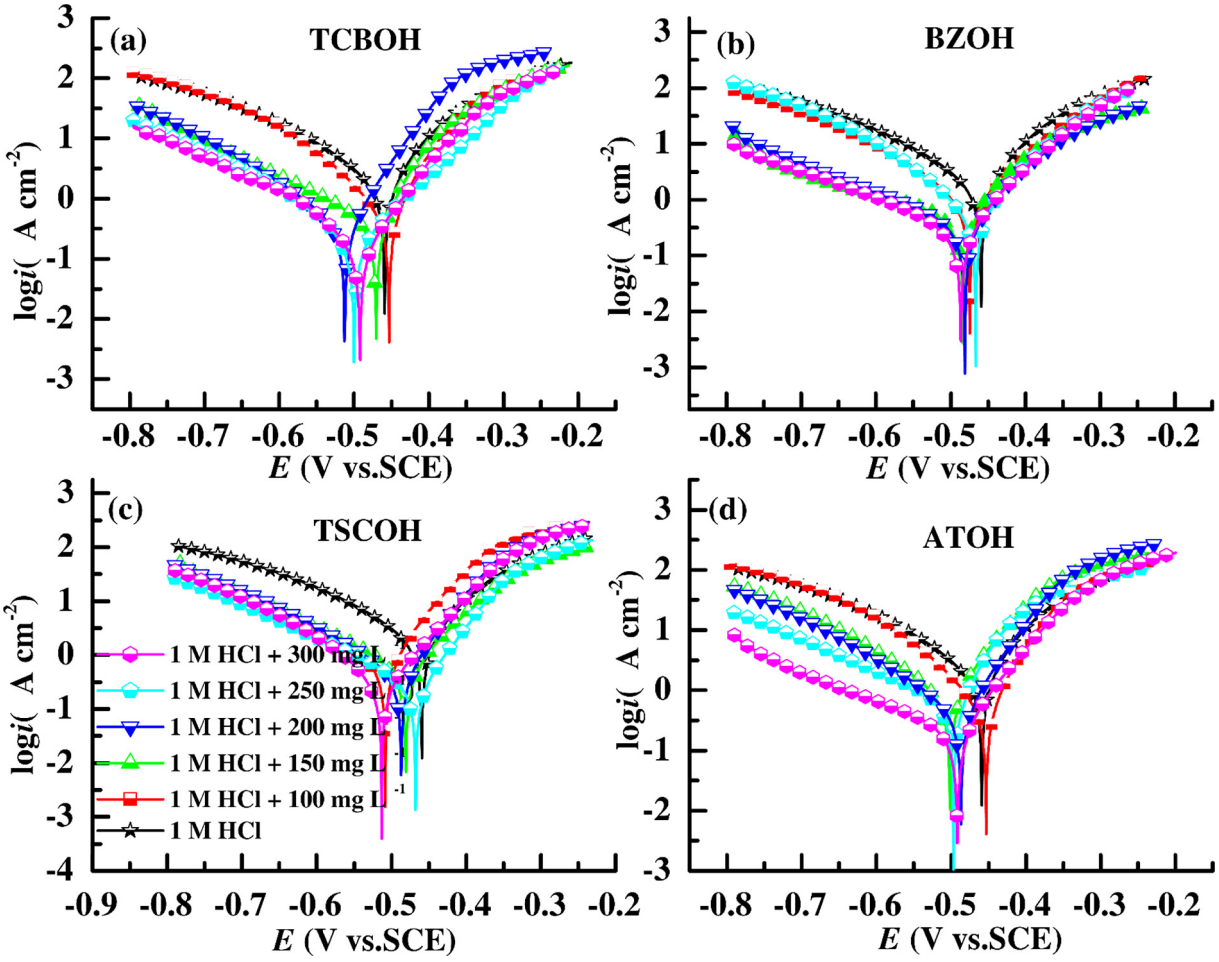

Fig. 7. Potentiodynamic polarization curves of MS obtained in 1 M HCl in absence and presence of (a) ATOH, (b) BZOH, (c) TSCOH, and (TCBOH).

$$C_R = \frac{RT}{Nh}\exp\left(\frac{\Delta S^*}{R}\right)\exp\left(-\frac{\Delta H^*}{RT}\right) \quad (19)$$

where all the parameters have their usual meaning in context to corrosion kinetics described elsewhere [54].

A plot of log C_R vs. $1/T$ (Fig. 8b) provides a straight line whose slope and intercept value enables us to calculate activation energy, E_a, and Arrhenius factor, λ. The linear regression coefficient ($R^2 \approx 1$) value affirms kinetic determination of corrosion and its inhibitory effect. The value of E_a, and λ thus attained are tabulated in Table 5. The value of both, E_a, and λ are enhanced in the presence of inhibitor which affirms hindrance to the corrosion process offered by inhibitor molecule [55].

According to Eq. (18), a high activation energy and low Arrhenius parameter value favours lowering of corrosion rate. The order of activation energy according to Table 5 is ATOH > TCBOH > TSCOH > BZOH > blank. ATOH's lowest effectiveness is associated with its high Arrhenius factor value.

The enthalpy and entropy of activation values can be known from the value of slope and intercept of straight line achieved by plotting log C_R/T vs. $1/T$ (Fig. 8c) and are given in Table 5. The negative value of ΔH^* is a result of association of inhibitor molecule with metal surface compared to dissolution process [56], lead to reduced metal corrosion. Though the value of ΔS^* was found negative in both conditions, however, presence of inhibitor raised the entropy of activation. Actually the adsorption of inhibitor and desorption of solvent occur simultaneously at the same time. Thus, the increased entropy is an outcome of desorption of water molecule from the metallic surface [57].

3.4.3. Adsorption behaviour of inhibitors

Application of inhibitors lowers the attack of aggressive species mainly by adsorbing themselves over metallic surface. The inhibitor molecules replaces aggressive species from metal surface and get adsorbed themselves competitively. Thus, understand of adsorption of inhibitor species is necessary to recognize the corrosion inhibitory mechanism. This could be potentially done by the study of adsorption isotherm.

The surface coverage, θ, for a concentration range used for this investigation was calculated as per Eq. (20).

$$\theta = \frac{w^a - w^i}{w^a} \quad (20)$$

Various standard adsorption isotherms (Frumkin, Temkin, Flory-Huggins and Langmuir) were attempted to fit surface coverage values, θ. By far, Langmuir isotherm (Eq. (21)) was found most fit because linear regression coefficient was closest to unity ($R^2 = 0.999$).

$$\frac{C_{inh}}{\theta} = \frac{1}{K_{ads}} + C_{inh} \quad (21)$$

where C_{inh} and K_{ads} are written for inhibitor's concentration and adsorption constant respectively.

A plot of C_{inh} vs. $\frac{C_{inh}}{\theta}$ (Fig. 8d) produces a straight line whose intercept enabled us to get the value of K_{ads} for different inhibitors, listed in Table 5.

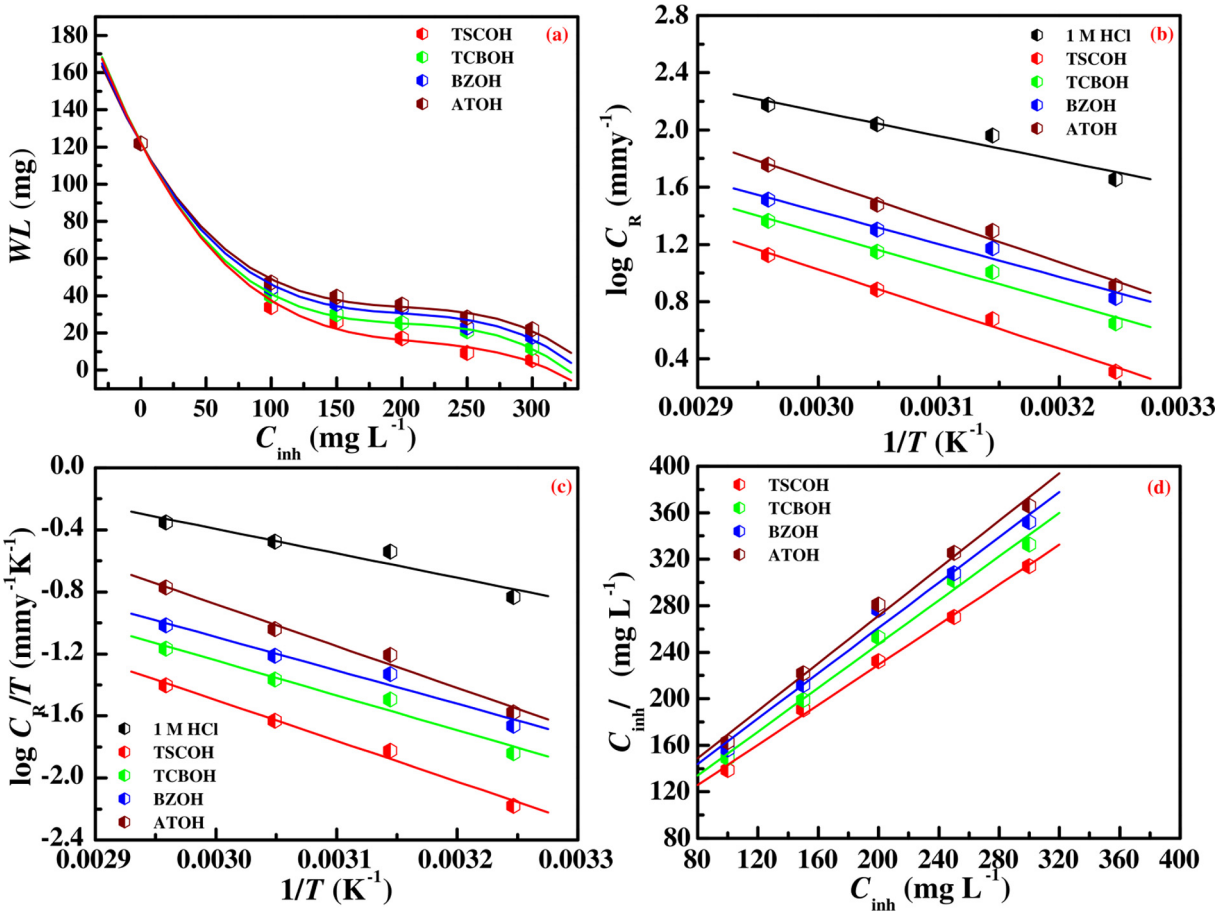

Fig. 8. (a) weight loss of MS against amount of inhibitor in acidic solution, (b) Arrhenius plot for log C_R vs. 1/T, (c) log C_R/T vs. 1/T, and (d) Langmuir isotherm.

Adsorption constant,K_{ads} enables the calculation of Gibb's free energy of adsorption,ΔG^o_{ads} (see Table 5) with the help of Eq. (22) as:

$$-0.018 \exp\left(\frac{-\Delta G^o_{ads}}{RT}\right) = K_{ads} \quad (22)$$

Where R and T have their usual meaning as described earlier [58].

The spontaneity of adsorption is reflected by negative value of Gibb's free energy of adsorption whereas extent of adsorption is determined by K_{ads}.

The values of K_{ads} and ΔG^o_{ads} can be further used to get the value of thermodynamic adsorption parameters with the help of Van't Hoff and Gibb's Helmholtz equations as [59]:

$$\frac{1}{55.5} + \frac{-\Delta H^o_{ads}}{RT} + \frac{\Delta S^o_{ads}}{R} = \ln K_{ads} \quad (23)$$

$$\Delta H^o_{ads} - T\Delta S^o_{ads} = \Delta G^o_{ads} \quad (24)$$

A straight line attained by plotting either lnK_{ads} vs. 1/T (Fig. 9a) or ΔG^o_{ads}vs. T (Fig. 9b) enabled us to calculate the value of ΔH^o_{ads}, and ΔS^o_{ads}. Both methods led to consistence result of ΔH^o_{ads}, and ΔS^o_{ads} (Table 5).

Generally, adsorption proceeds with negative enthalpy or heat of adsorption,ΔH^o_{ads}, which must be further associated with decrease in entropy or ordering of adsorbing species. But, here in this study, both ΔH^o_{ads}, andΔS^o_{ads}values are positive which is related to substitutional adsorption of inhibitor which get adsorbed themselves replacing water molecules (solvent) [60].

3.5. Topographical study of MS surface

3.5.1. SEM

The role of adsorption of tested inhibitors on the surface morphology of working electrodes have been investigated by capturing SEM images,

Table 5
Thermodynamic activation and adsorption parameters obtained for mild steel in HCl.

Name of inhibitor	E_a (kJ mol^{-1})	λ (mg cm^{-2})	ΔH^* (kJ mol^{-1})	ΔS^* (J K^{-1} mol^{-1})	K_{ads} (mol^{-1})	ΔH^o_{ads} [a] (kj mol^{-1})	ΔS^o_{ads} [a] (J K^{-1} mol^{-1})	ΔH^o_{ads} [b] (kj mol^{-1})	ΔS^o_{ads} [b] (J K^{-1} mol^{-1})	$-\Delta G^o_{ads}$ (kj mol^{-1})	R_L
–	33.04	2.03×10^7	30.14	−114.76	–	–	–	–	–	–	–
ATOH	54.45	1.50×10^{10}	51.64	−59.52	0.29×10^4	21.54	44.20	22.65	43.70	30.71	0.18
BZOH	44.07	2.18×10^8	41.22	−94.83	0.48×10^4	14.72	58.63	16.45	58.30	32.04	0.14
TSCOH	45.90	2.98×10^8	43.05	−92.24	0.63×10^4	13.49	60.44	15.20	60.10	32.72	0.09
TCBOH	53.10	2.22×10^9	50.31	−75.33	1.58×10^4	29.43	4.74	32.10	3.78	35.04	0.04

[a] Calculated from Eq. (23).
[b] Calculated from Eq. (24).

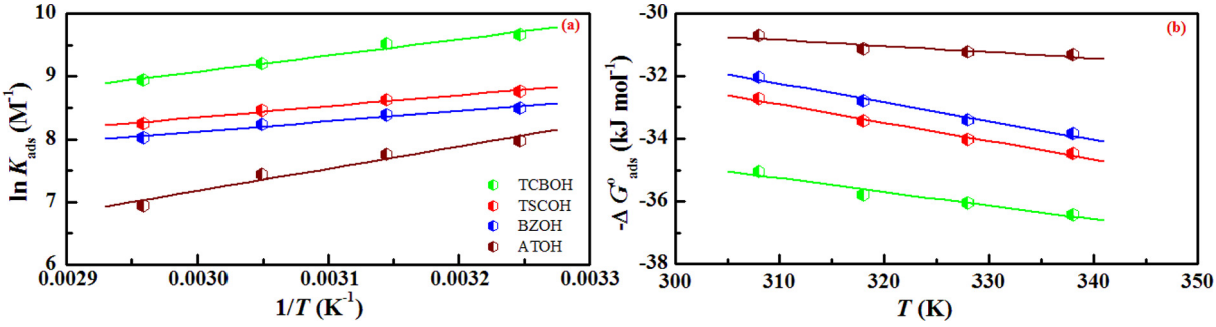

Fig. 9. (a) plot of ln K_{ads} vs. 1/T, and (b) ΔG^{o}_{ads} vs. T.

presented as Fig. 10a-f, of MS surfaces dipped in different acid solutions. Fig. 10a shows smooth MS surface before immersion in electrolytic solution which changed in to a highly degraded rough surface (Fig. 10b) when dipped in mere acid solution without adding any inhibitor. This deteriorated roughened surface of MS is due to attack of highly corrosive acid ions. Addition of inhibitor to acid solution prevents attack of corrosive species on MS surface and thereby resulted in to comparatively smoother surfaces (Fig. 10c-f). A highly smooth, not attacked MS surface (Fig. 10f) resulted when dipped in to acid + TCBOH solution. It is related to excellent efficiency of TCBOH compared to other tested inhibitors.

3.5.2. AFM

The effect of incorporation of inhibitors to the acid solution on MS surface could be visibly observed by using AFM technique as it helps to study change in the surface morphology at nano level [61].

The MS surfaces, dipped in different electrolytic solutions, were analysed by AFM and compared these AFM data with those obtained for MS surface before immersion in any solution. 2D AFM images along with longitudinal cross section graphs as well as 3D AFM images of MS surfaces before exposure to corrosive solution and after exposure to different acid solutions are illustrated as Figs. 11 and 12. These AFM images were analysed by software Nanoscope 1.8 and obtained different useful AFM parameters viz. average roughness (R_a), root-mean-square roughness (R_q), and maximum peak to valley height (R_{p-v}) are enlisted in Table 6.

Inspection of Table 6 illustrates that these parameters are lowest for unexposed MS surface while it increased by maximum extent for MS surface exposed directly to 1 M HCl. Application of inhibitors to the acidic solution controls the corrosion rate by adsorbing themselves on MS surface replacing corrosive ions. This fact can be viewed by AFM parameters obtained for MS surface dipped in different inhibitor solutions. The order of the value of AFM parameters are 1 M HCl > ATOH > BZOH > TSCOH > TCBOH > unexposed MS. This order of corrosion inhibition is supported by the results obtained from all other methods. This corrosion control by addition of inhibitors is due to the development of inhibitor layer on the MS surface.

3.5.3. XPS

The XPS spectra of the film adsorbed on the MS (Fig. 13) comprises of several peaks for various elements such as C 1 s, O 1 s, Fe2p, N 1 s and S 2p which affirms the adsorption of an inhibitor on the MS.

The deconvoluted C 1 s spectrum depicted three peaks i.e. 285 eV, 286.3 eV, and 288.1 eV. The primary peak located at 285 eV may be attributed to the C–C, C=C, and C–H bonds [62], whereas the peak at 286.3 eV may be linked to the C=N and C=S bond in the inhibitor

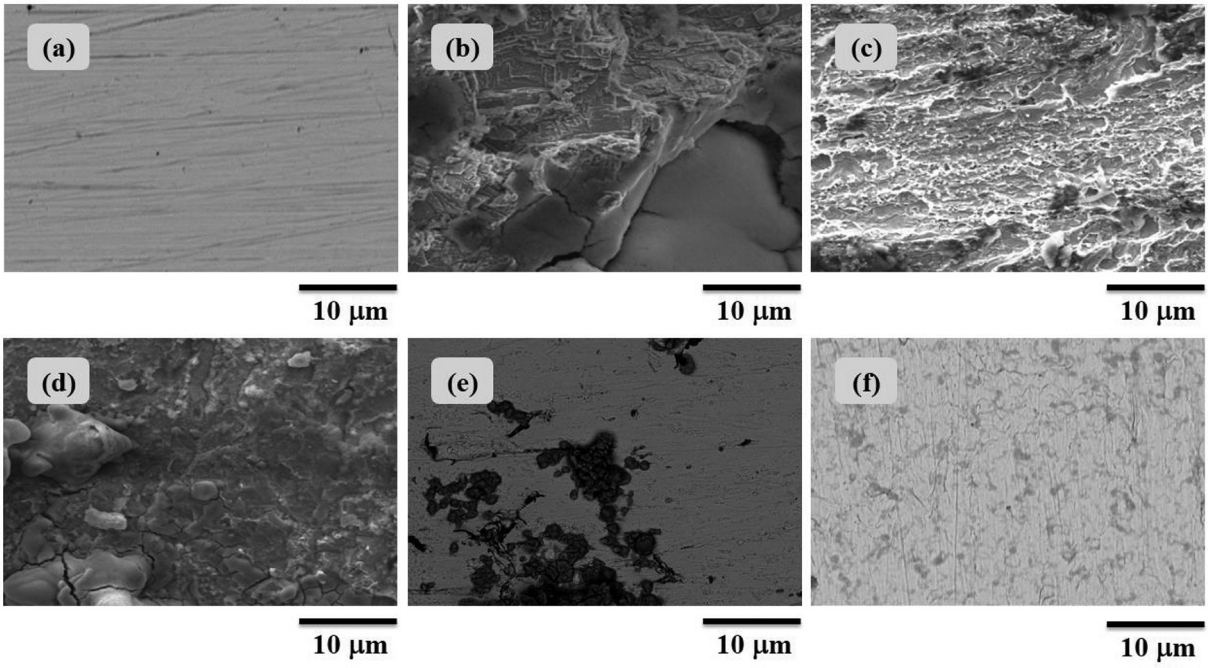

Fig. 10. SEM images of MS (a) before immersion in acid solution, (b) after immersion in 1 M HCl, (c) after immersion in 1 M HCl + 300 mg L^{-1}ATOH, (d) 1 M HCl + 300 mg L^{-1}BZOH, (e) 1 M HCl + 300 mg L^{-1}TSCOH, and (f) 1 M HCl + 300 mg L^{-1}TCBOH.

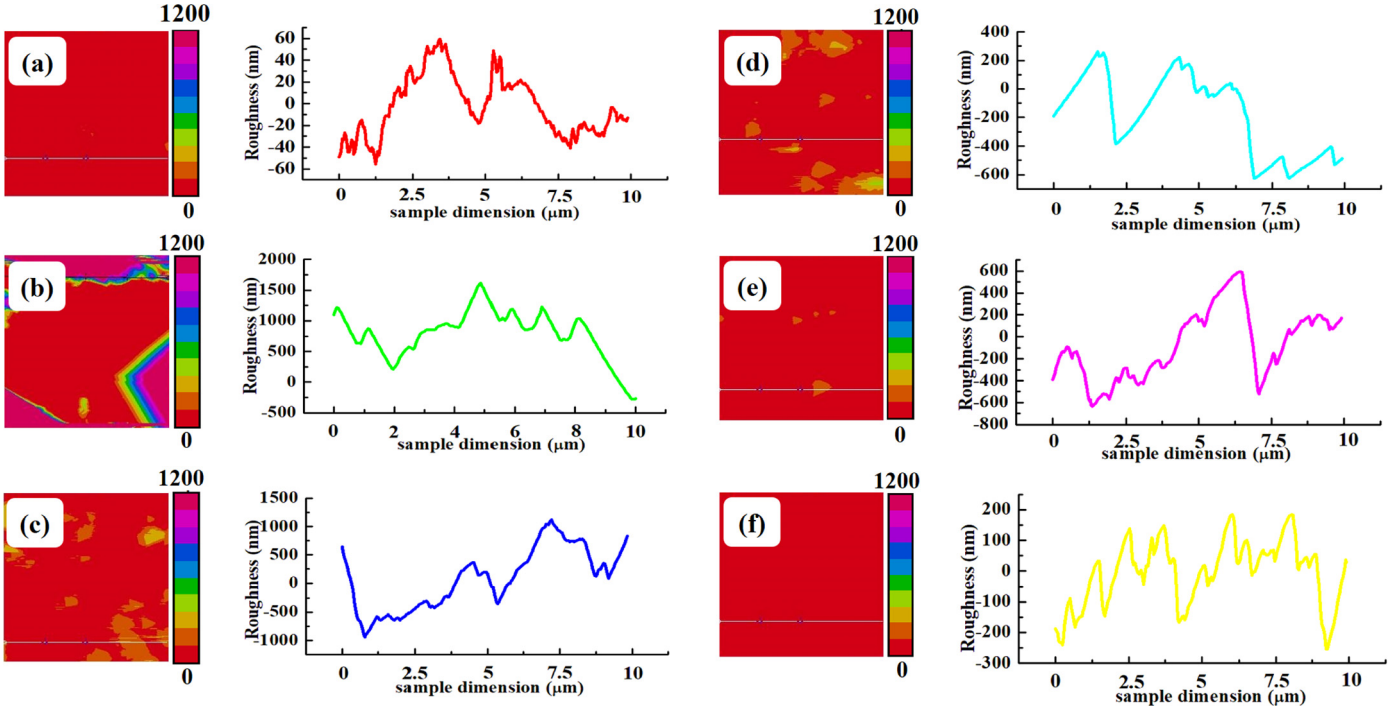

Fig. 11. 2D AFM images and longitudinal section images the MS surface (a) before immersion in acid solution, (b) after immersion in 1 M HCl, (c) after immersion in 1 M HCl + 300 mg L^{-1} ATOH, (d) 1 M HCl + 300 mg L^{-1} BZOH, (e) 1 M HCl + 300 mg L^{-1} TSCOH, and (f) 1 M HCl + 300 mg L^{-1} TCBOH.

moiety. The third peak located at 288.1 eV is attributed to C=N^+. This contribution of C=N^+ for this peak is resulted either from the protonation of the C=N bond and/or due to coordination of N with the mild steel surface [63].

O 1 s spectra exhibited three peaks at B.E 529.8 eV, 531.5 eV, and 533.5 eV. The peaks at 529.8 eV and 531.5 eV may be attributed for oxygen atom in O^{2-} state coordinated with Fe^{3+} (Fe_2O_3 or Fe_3O_4) and hydroxide species (FeOOH) respectively [64]. Peak obtained at 533.5 eV is result of adsorption of water molecules moisture on MS surface [65].

Deconvolution of Fe2p spectra resulted in peaks located at 710 eV, 713 eV, 719 eV and 725 eV. The primary peak at 710 eV is ascribed to Fe_2O_3 (i.e., Fe^{3+} oxide) and FeOOH (i.e., oxyhydroxide). The peak observed at 713 eV indicates the existence of $FeCl_3$ on the MS surface

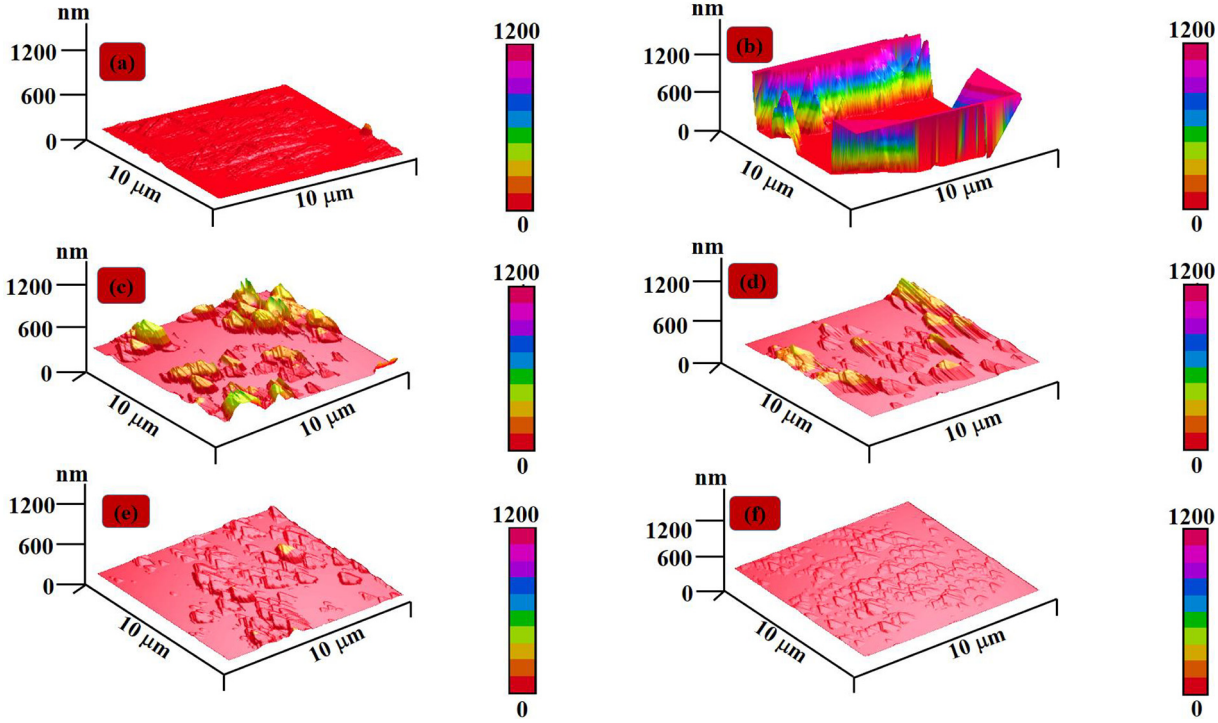

Fig. 12. 3D AFM images of MS surface before immersion in acid solution, (b) after immersion in 1 M HCl, (c) after immersion in 1 M HCl + 300 mg L^{-1} ATOH, (d) 1 M HCl + 300 mg L^{-1} BZOH, (e) 1 M HCl + 300 mg L^{-1} TSCOH, and (f) 1 M HCl + 300 mg L^{-1} TCBOH.

Table 6
AFM results obtained for mild steel in HCl solution in absence and presence of inhibitors.

Sample	R_a (nm)	R_q (nm)	$R_{p\text{-}v}$ (nm)
MS before immersion	30.2	38.2	155
MS/1 M HCl	1335	1822	3714
MS/1 M HCl + ATOH	231	279	1622
MS/1 M HCl + BZOH	140	171	872
MS/1 M HCl + TSCOH	75.6	102	795
MS/1 M HCl + TCBOH	54.4	70.2	541

because of HCl corrosive solution [66]. The peak seen at 719 eV is attributable of Fe (III) satellite. The peak at 725 eV can be due to $Fe2p_{1/2}$ representative of the iron in the form of Fe_2O_3 and FeOOH [67].

Deconvolution of N 1 s may be result into three peaks i.e. 399 eV, 400.5 eV and 402 eV. The primary peak at 399 eV is correspondent to the unprotonated nitrogen atoms (=N- moiety), whereas the peak at 400.5 is a result of N—Fe bond attributable to the bonding of nitrogen in the inhibitor with the iron in the MS. The peak at 402 eV is because of nitrogen in the oxidized state existing because of the protonation of nitrogen that allows a positive polarization of the N atom [68].

The S 2p XPS spectra represented peaks located at 162 eV and 168.5 eV. The first peak at around 162 eV may be because of disulfide species, i.e. FeS_2 while the peak situated at 168.5 eV is attributed to sulfur bonded to Fe to result into S — Fe complex [69].

3.6. Theoretical assessment

3.6.1. Solubility and toxicity analysis

As shown in Fig. 14a, we can see that all the four compounds possess excellent water solubility in strong acid solution, which can be attributed to the hydroxyl, amino, and imine groups in their structures. Therefore, they can behave as potential water soluble corrosion inhibitors for MS in acid medium. Also, as depicted in Fig. 14b, several typical toxicity descriptors including carcinogenicity, biodegradability, and sensitization were given to represent the toxicities. Generally, probability values lying within 0.0 to 0.3 are thought to be low probabilities, and are anticipated to give a negative response in an experimental assay; whereas probability values with more than 0.7 are very high, and are expected to give a positive response in an experimental assay. Probabilities more than 0.3 but lower than 0.7 are treated indeterminate. Careful examination of the attained probability values in Fig. 14b one could conclude that the toxic level of involved inhibitors is very low (all less than 0.09), and thus these compounds are environmentally friendly.

3.6.2. Natural bond orbital (NBO) analysis

Table S1 displays the essential intramolecular interactions for **ATOH, BZOH, TSCOH and TCBOH** compounds calculated at B3LYP/6–311++G (2df,2pd) level in the water phase. Accordingly, the LP(2) O11 → π* C2-C3 (2) and the LP(2) O11 → π* C2-C3 (2) interactions have a vital role in stabilization of all compounds: the perturbative energy of these interactions is calculated at 27.15 and 24.86 kcal/mol for **ATOH**, 27.44 and 23.77 kcal/mol for **BZOH**, 27.26 and 24.84 kcal/mol **TSCOH**, and 27.79 and 24.84 kcal/mol for **TCBOH**, respectively. Furthermore, the π → π* interactions have greatly affected the stabilization energy for all compounds and the calculated $E^{(2)}$ values for the saturated ring of these compounds are almost similar to each other. For instance, the resonance energy for π C1-C6 (2) → π* C2-C3 interaction of **ATOH, BZOH, TSCOH and TCBOH compounds** is calculated in 22.61, 22.67, 22.76 and 23.03 kcal/mol, respectively. Although its contribution to the stabilization energy is lower than the other interactions, the hyperconjugative interaction energy is worth to mention here. Namely, this energy for σ C14-H15 (1) → π* C13-N18 (2) interaction for **ATOH, BZOH, TSCOH and TCBOH compounds** has estimated in 4.32 (ED_i = 1.97179e), 4.09

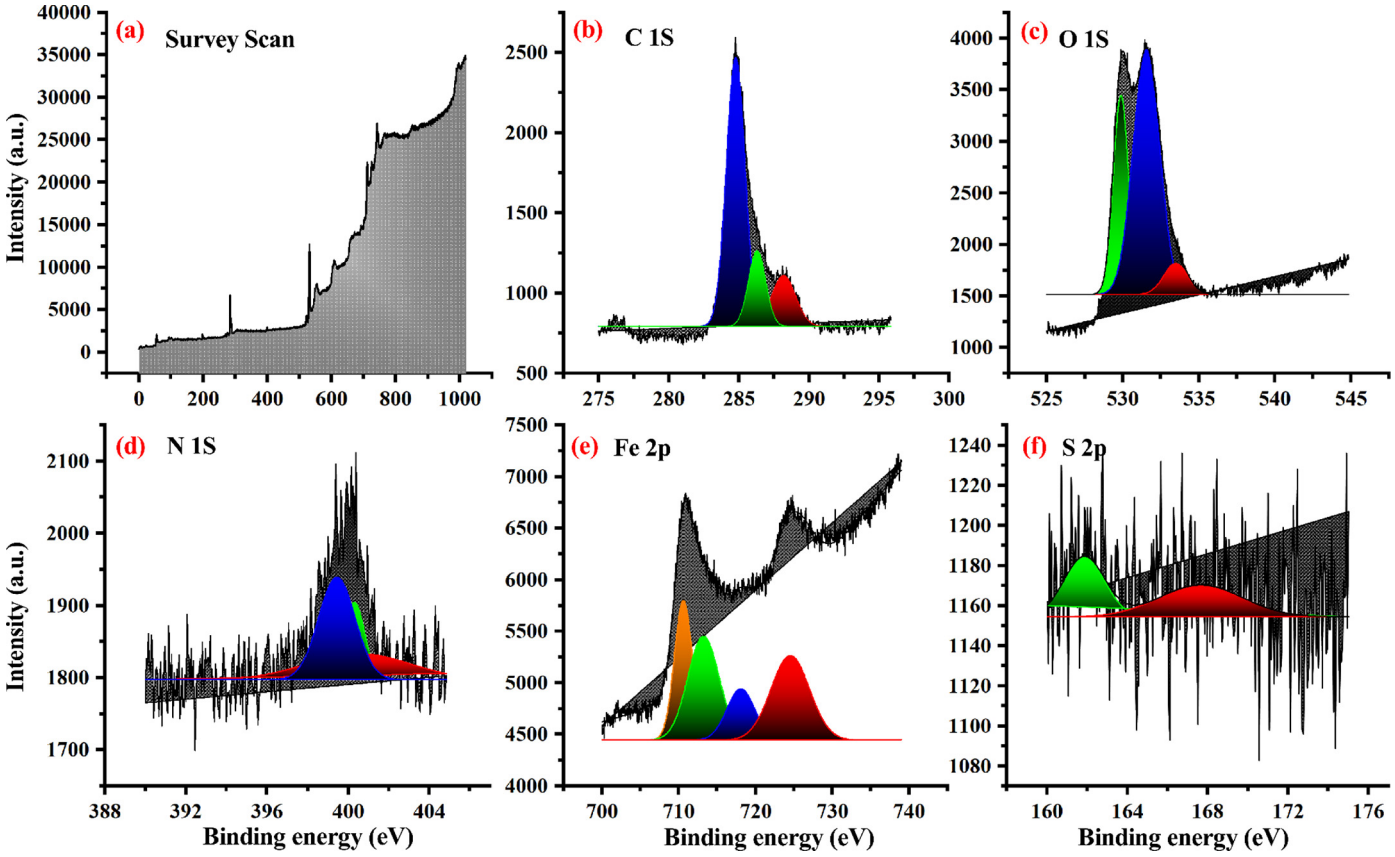

Fig. 13. XPS spectra of mild steel surface removed after immersion in 1 M HCl solution with 300 mg L^{-1} of TCBOH: (a) survey scan, (b) narrow scan spectra of C, (c) O, (d) N, (e) Fe, and (f) S.

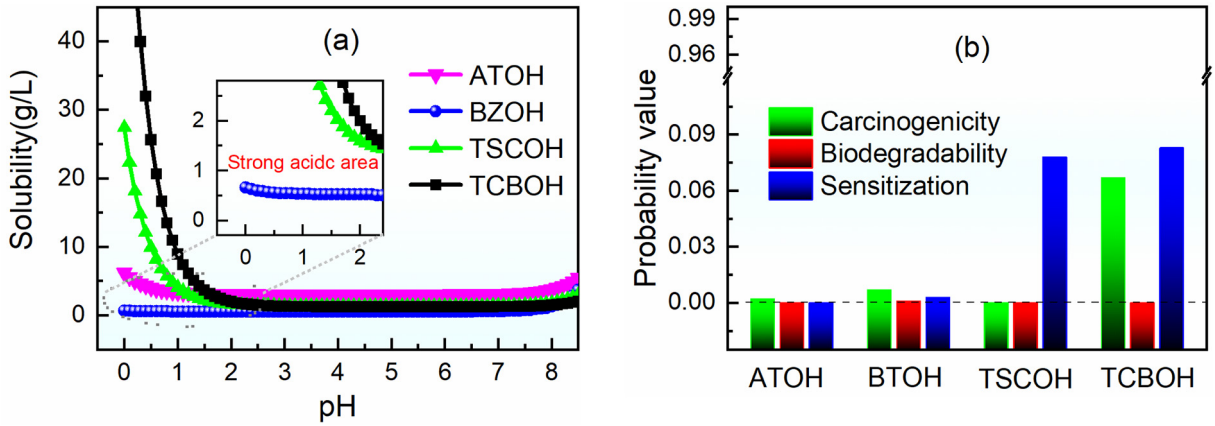

Fig. 14. (a) The solubility and (b) toxicity assessments for the studied inhibitors.

(ED_i = 1.97179e), 4.09 (ED_i = 1.97179e) and 3.84 kcal/mol (ED_i = 1.97179e), orderly. On the other hand, the energies of σ C23-H24 (1) → π* C13-N18 (2) and σC23-H24 (1) → π* C13-N18 (2) interactions for **ATOH** compound are calculated in 5.59 and 4.92 kcal/mol, respectively, since this compound has an additional methyl group attached to aliphatic part of the compound. Moreover, the π → π* interactions for **BZOH** compound have calculated in 15.43–22.12 kcal/mol contributed to the perturbative energy, remarkable. It is apparent that the –(C=S)-NH_2 and -(C=S)-N-NH_2 substituent groups for **TSCOH and TCBOH compounds** have no important contribution to the perturbative energy. These interactions and their quantities have an effect on the chemical reactivity behaviour of the investigated compounds.

Fig. 15 demonstrates the HOMO& LUMO and MEP graphs for **ATOH**, **BZOH**, **TSCOH** and **TCBOH** compounds. For the **ATOH** and **BZOH** compounds, HOMO is expanded over the whole molecular surface except for the -CH_3 for **ATOH** and phenylic group for **BZOH** while the HOMO is distributed on –(C=S)-NH_2 for **TSCOH** and on -(C=S)-N-NH_2 for **TCBOH**. As known well, the HOMO indicates the nucleophilic attack site for the interested molecules. In this context, the -CH_3 for **ATOH**, the phenylic group for **BZOH**, hydroxyphenyl and -CH_3 groups for **TSCOH** and **TCBOH** compounds have no essential role in the nucleophilic attack reactions. On the other hand, LUMO plots reveal that the -OH group for all compounds has no effective role for the electrophilic attacks because of no electron density on this group for all compounds.

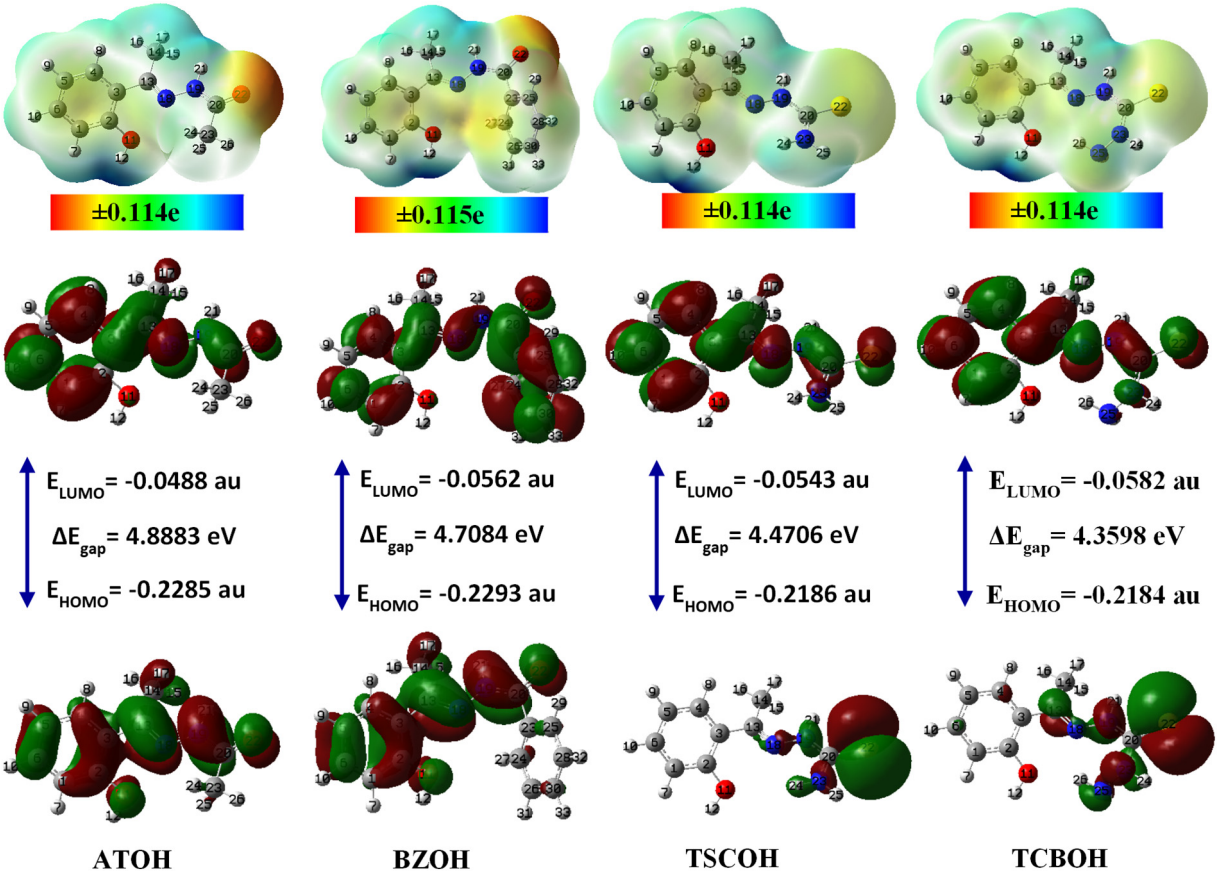

Fig. 15. HOMO& LUMO (isoval:0.02) and MEP (isoval:0.0004) pilots of ATOH, BZOH, TSCOH and TCBOH compounds, at B3LYP/6–311++G(2df,2pd) level in the water phase.

Besides, the -CH_3 group for the **ATOH** and -NH_2 group for **TCBOH** have also no active role in the electrophilic attack reactions. In addition, the red color density on oxygen atom (=O) around for **ATOH** and **BZOH** compounds implies the electron-rich region whereas the blue color over the hydrogen atom of hydroxyl group indices the electron-poor site. Also, for **TSCOH** and **TCBOH** compounds, the similar H atom around implies the region of positive electrostatic potential, whereas the orange color over sulfur atom implies the negative electrostatic potential region in medium size for these compounds.

Frontier orbital energies are extensively used in the theoretical estimation of corrosion inhibition performances of molecules. It is significantly noticeable that HOMO orbital energy describes the electron donating tendency of molecules while LUMO orbital energy gives clues about electron accepting ability of molecules. Molecules having high E_{HOMO} values act as good corrosion inhibitors. Calculated frontier orbital energies presented in Table 7 show that corrosion inhibition performances of studied molecules obeys the order TCBOH > TSCOH > BZOH > ATOH. It is apparent that this ranking is very compatible experimental results. Hard and Soft Acid Base Principle (HSAB) introduced by Pearson [70] classifies the chemical species as hard and soft. Hard molecules possess higher HOMO-LUMO energy gap values. On the other hand, energy gap values of soft compounds are quite low. For that reason, quantities like hardness, softness as well as energy gap are closely related each other. Chemical hardness [71] is known as the resistance towards electron cloud polarization or detachment of atoms, ions and molecules. In accordance to the Maximum Hardness Principle [72] "there seems to be a rule of nature that molecules arrange themselves so as to be as hard as possible." This means that chemical hardness is a measure of the stability and hard substances are more stable in contrast to the soft ones. As can be seen from the definition given above of chemical hardness that hard molecules are not efficient against the corrosion of metallic surfaces. According to determined hardness, softness and energy gap values, one can say that corrosion inhibition efficiency order for investigated molecules is stated as TCBOH > TSCOH > BZOH > ATOH. This theoretical data are in good correlation with experimentally obtained results.

Electronegativity is known as electron abstracting power of chemical molecules and this quantity signifies the electron accepting capability of inhibitor molecules. Good corrosion inhibitors give easily electrons to metal surfaces and they have low electronegativity values in general. The electronegativity values of studied molecules presented in Table 7 indicate that TCBOH and TSCOH molecules have the lowest value of the electronegativity. As noted in the previous part, Parr's electrophilicity index is related with electronegativity and hardness of chemical species. Minimum Electrophilicity Principle [73] defines that the natural direction of a chemical reaction is towards a state of minimum electrophilicity, or in other words the molecules having lower electrophilicity values are more stable in comparison to others. It is apparent from the results given that the most stable inhibitor molecule is ATOH while the most reactive one is TCBOH. Within the framework of calculated electrophilicity values, the corrosion combating ability order of investigated inhibitors can be written as: TCBOH > TSCOH > BZOH > ATOH. This ranking supports the experimental data. Molecules with high polarizability and dipole moment are good corrosion inhibitors. Minimum Polarizability Principle [74] introduced encouraged by Maximum Hardness Principle signifies that in a stable state polarizability (α) is reduced. In the study, it is clear that the most polarized molecules among studied compounds are BZOH and TCBOH. Few researchers noted that dipole moment is a vital parameter for corrosion inhibition analysis while some authors said it should not be considered in corrosion analysis. It is significant to notice that our dipole moment data support the usefulness of dipole moment in such studies. ΔN values given in related table can be widely used in the prediction of corrosion inhibition activities. This value represent the transferred electron amount between inhibitor molecule and metal surface. Corrosion inhibition performances of molecules increase as their ΔN values increase. Calculated ΔN values given in Table 7 show that corrosion inhibition performances of the molecules obey the order: TCBOH > TSCOH > BZOH > ATOH. The ranking is compatible with experimental order.

3.6.3. Molecular dynamics simulation

The dynamics procedure was performed and the complete system approached equilibrium till both temperature as well as energy of the system are balanced. The low energy adsorption configurations of four inhibitors adsorbed onto Fe (110) surface are represented in Fig. 16. Fig. 16 represents that the adsorption centers of inhibitors on the Fe (110) surface are the electrons of aromatic rings, O, N, and S atoms. The inhibitor molecules adsorbed almost flat orientation on the Fe surface to enhance surface coverage and contact, leading to a stronger coordination for adsorbate/substrate system.

Table 7
The quantum chemical reactivity identifiers of ATOH, BZOH, TSCOH and TCBOH compounds.

	Gas											
	631G(d,p)				6311 + G(d,p)				6311++G(2df,2pd)			
	ATOH (1)	BZOH (2)	TSCOH (3)	TCBOH (4)	ATOH (1)	BZOH (2)	TSCOH (3)	TCBOH (4)	ATOH (1)	BZOH (2)	TSCOH (3)	TCBOH (4)
HOMO (−I)	−0.2117	−0.2143	−0.2003	−0.2002	−0.2285	−0.2300	−0.2127	−0.2141	−0.2278	−0.2295	−0.2124	−0.2107
LUMO (−A)	−0.0363	−0.0448	−0.0485	−0.0519	−0.0505	−0.0584	−0.0617	−0.0651	−0.0505	−0.0573	−0.0613	−0.0644
ΔE (L-H)	4.7742	4.6131	4.1304	4.0341	4.8447	4.6697	4.1089	4.0559	4.8259	4.6861	4.1127	3.9808
$\mu = -(I + A)/2$	−3.3735	−3.5248	−3.3839	−3.4293	−3.7965	−3.9248	−3.7339	−3.7980	−3.7858	−3.9023	−3.7236	−3.7431
$\eta = (I-A)/2$	2.3871	2.3066	2.0652	2.0170	2.4224	2.3349	2.0545	2.0279	2.4130	2.3430	2.0564	1.9904
$\omega = \mu^*\mu/2\eta$	2.3838	2.6933	2.7723	2.9152	2.9751	3.2988	3.3932	3.5566	2.9698	3.2495	3.3713	3.5196
$\Delta N = -\mu/\eta$	1.4132	1.5282	1.6385	1.7002	1.5673	1.6810	1.8175	1.8729	1.5689	1.6655	1.8108	1.8806
D (debye)	4.6029	4.7331	6.8398	7.0633	5.0603	5.0473	6.7168	6.9002	4.9356	4.9167	6.5522	6.7501
α (au)	134.2220	185.5297	155.8550	161.6393	152.3950	210.8720	180.0797	187.8340	155.4503	213.9123	184.0643	191.9057
	Water											
	ATOH (1)	BZOH (2)	TSCOH (3)	TCBOH (4)	ATOH (1)	BZOH (2)	TSCOH (3)	TCBOH (4)	ATOH (1)	BZOH (2)	TSCOH (3)	TCBOH (4)
HOMO (−I)	−0.2140	−0.2156	−0.0207	−0.2082	−0.2296	−0.2304	−0.2196	−0.2195	−0.2285	−0.2293	−0.2186	−0.2184
LUMO (−A)	−0.0376	−0.0470	−0.0431	−0.0469	−0.0497	−0.0579	−0.0551	−0.0594	−0.0488	−0.0562	−0.0543	−0.0582
ΔE (L-H)	4.8020	4.5857	−0.6086	4.3895	4.8961	4.6940	4.4779	4.3574	4.8883	4.7084	4.4706	4.3598
$\mu = -(I + A)/2$	−3.4231	−3.5729	−0.8680	−3.4701	−3.7994	−3.9236	−3.7378	−3.7937	−3.7723	−3.8840	−3.7129	−3.7628
$\eta = (I-A)/2$	2.4010	2.2928	−0.3043	2.1947	2.4481	2.3470	2.2390	2.1787	2.4441	2.3542	2.2353	2.1799
$\omega = \mu^*\mu/2\eta$	2.4401	2.7837	−1.2379	2.7433	2.9483	3.2797	3.1199	3.3029	2.9111	3.2040	3.0836	3.2475
$\Delta N = -\mu/\eta$	1.4257	1.5583	−2.8524	1.5811	1.5520	1.6718	1.6694	1.7413	1.5434	1.6498	1.6610	1.7261
D (debye)	6.9616	7.0325	9.4860	9.8167	7.8668	7.8278	9.6412	9.9065	7.7161	7.6923	9.4808	9.7468
α (au)	188.4700	262.0247	210.9500	223.6223	218.8623	306.0313	252.5450	270.3927	225.0167	313.2373	260.9693	278.4997

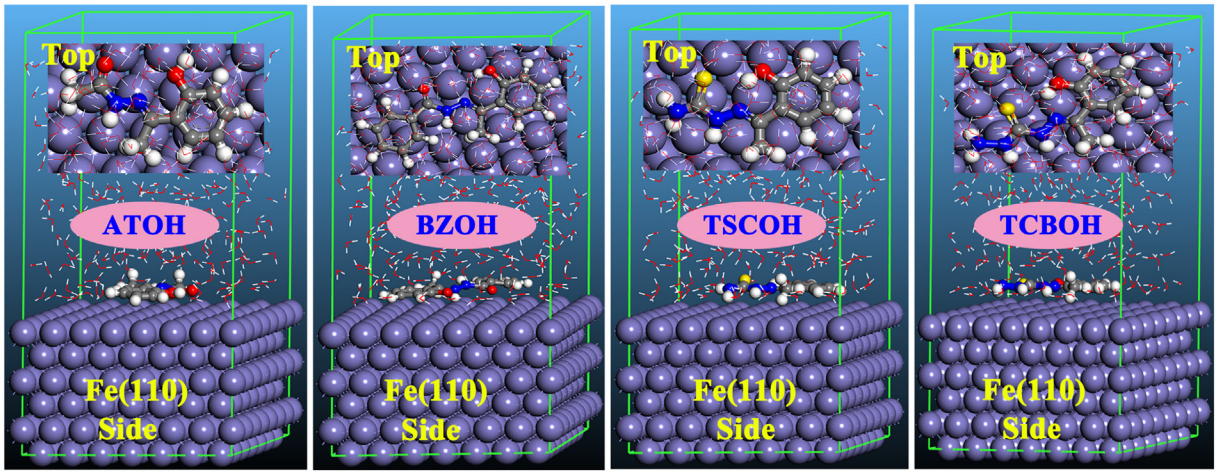

Fig. 16. Side and top views of most stable adsorption configurations for four inhibitors on Fe (110) surface.

The performance of corrosion inhibitors absorbed on Fe surface can be formulated by an adsorption energy (E_{ads}). The adsorption energy in a solution could be determined using the subsequent equations:

$$E_{ads} = E_{total} - (E_{surf+water} + E_{inh+water}) + E_{water} \quad (25)$$

where, E_{total} is the complete potential energy of the system, which comprises iron crystal, the.

adsorbed inhibitor and solution; $E_{surf+water}$ and $E_{inh+water}$ denotes the potential energies of the system with no inhibitor and the system with no iron crystal, respectively; E_{water} is the potential energy of the water molecules.

The adsorption energies in this work were compute from the average adsorption energy of the attained equilibrium configurations. The determined E_{ads} values are −473.1, −475.4, −477.9, and − 489.4 kJ mol^{-1} for ATOH, BZOH, TSCOH, and TCBOH, respectively. We can see that the adsorption energies are negative and thus spontaneous adsorption could be anticipated. The larger E_{ads} value signifies the stronger interaction among the inhibitor and metallic surface. Clearly, it appears that TCBOH has more absolute values of E_{ads} than the other three inhibitors, and therefore it presented the best inhibiting action for carbon steel, which is in correlation with the experimental results.

4. Conclusion

1. This study infers that hydroxy acetophenone derivatives (ATOH, BZOH, TSCOH and TCBOH) improves the corrosion resistance of mild steel extensively by adsorb themselves in best suitable orientation.
2. Their efficient adsorption results in to film formation which is well proven by a variety of microscopic studies viz., SEM, AFM, and XPS.
3. Tafel polarization results show that the hydroxy acetophenone derivatives simultaneously restrict the cathodic and anodic reactions (though the effect on cathodic reactions are more pronounced) which proves their mixed type nature.
4. Ab initio DFT results revealed the inhibitor's ability for electron sharing with the suitable metal d-orbitals that might facilitate its adsorption on the metal surface.
5. The theoretical result infers the non-toxic nature and high solubility of the inhibitors in acidic medium.

Author contributions

All authors have read and agreed to the published version of the manuscript.

Declaration of Competing Interest

There are no conflicts to declare.

Acknowledgements

Authors BC and ST are thankful to the Netaji Subhas University of Technology, New Delhi for providing financial assistance to carry out the experimental work. Author AKS, MS and BP are thankful to their institutions for providing work platform. The theoretical study of this project was sponsored by the National Natural Science Foundation of China (2176195).

Appendix A. Supplementary data

Supplementary data to this article can be found online at https://doi.org/10.1016/j.molliq.2021.115605.

References

[1] J.L. Lovell, Y.M. Rowan, Culture, Chronology and the Chalcolithic Theory and Transition, Oxford Press, 2011 ISBN 978–1–84217-993-2.
[2] W. Little, Introduction to Sociology, 2nd, Canadian edition, 2012.
[3] The Major Epochs and Phases of Maganese Accumulation in the Earth's History, Isotope Geochemistry2017 353–383, https://doi.org/10.1016/B978-0-12-803165-0.00004-5.
[4] K.P. Balan, Corrosion, Metallurgical Failure Analysis, 2018 155–178.
[5] J. Van Muylder, Thermodynamics of corrosion, in: J.O. Bockris, B.E. Conway, E. Yeager, R.E. White (Eds.), Electrochemical Materials Science. Comprehensive Treatise of Electrochemistry, 4, Springer, Boston, MA, 1981.
[6] www.corrotherm.co.uk/blog/the-advantage-of-using-metal-alloys-over-pure-metals-in-the-oil-and-gas.
[7] Z.T. Khodair, A.A. Khadom, H.A. Jasima, Corrosion protection of mild steel in different aqueous media via epoxy/nanomaterial coating: preparation, characterization and mathematical views, J. Mater. Res. Technol. 8 (2019) 424–435.
[8] A.K. Singh, M.A. Quraishi, The effect of some bis-thiadiazole derivatives on the corrosion of mild steel in hydrochloric acid, Corros. Sci. 52 (2010) 1373–1385.
[9] A.A. Nkuna, E.D. Akpan, I.B. Obot, C. Verma, E.E. Ebenso, L.C. Murulana, Impact of selected ionic liquids on corrosion protection of mild steel in acidic medium: experimental and computational studies, J. Mol. Liq. 314 (2020) 113609.
[10] A.K. Singh, M.A. Quraishi, Adsorption properties and inhibition of mild steel corrosion in hydrochloric acid solution by ceftobiprole, J. Appl. Electrochem. 41 (2011) 7–18.
[11] A.K. Singh, M.A. Quraishi, E.E. Ebenso, Inhibitive effect of cefuroxime on the corrosion of mild steel in hydrochloric acid solution, Int. J. Electrochem. Sci. 6 (2011) 5676–5688.
[12] H. Al-Sehaibani, Evaluation of extracts of henna leaves as environmentally friendly corrosion inhibitors for metals, Mater. Sci. Eng. Technol. 31 (2000) 1060–1063.
[13] I.H. Farooqi, Aqbal Hussain, P.A. Saini, M.A. Quraishi, Study of low cost eco-friendly compounds as corrosion inhibitors for cooling systems, Anti Corros. Method. M 46 (1999) 328–335.
[14] G. Bahlakeh, B. Ramezanzadeh, A. Dehghani, M. Ramezanzadeh, Novel cost-effective and high-performance green inhibitor based on aqueous *Peganum harmala* seed

extract for mild steel corrosion in HCl solution: detailed experimental and electronic/atomic level computational explorations, J. Mol. Liq. 283 (2019) 174–195.
[15] S. Marzorati, L. Verotta, S.P. Trasatti, Green corrosion inhibitors from natural sources and biomass wastes, Molecules. 24 (2019) 48–72.
[16] S.K. Ahmed, W.B. Ali, A.A. Khadom, Synthesis and investigations of heterocyclic compounds as corrosion inhibitors for mild steel in hydrochloric acid, Int. J. Ind. Chem. 10 (2019) 159–173.
[17] A.E. Vazquez, F.J. Rodriguez-Gomez, I.K. Martinez-Cruz, D. Angeles-Beltran, G.E. Negron-Silva, M. Palomar-Pardave, L.L. Romero, D. Perez-Martinez, A.M. Navarrete-Lopez, Adsorption and corrosion inhibition behaviour of new theophylline–triazole-based derivatives for steel in acidic medium, R. Soc. Open Sci. 6 (2019) 181738.
[18] C. Verma, D.K. Verma, E.E. Ebenso, M.A. Quraishi, Sulfur and phosphorus heteroatom-containing compounds as corrosion inhibitors: an overview, Heteroat. Chem. 29 (2018), e21437, .
[19] A.Y. Musa, R.T. Jalgham, A.B. Mohamad, Molecular dynamic and quantum chemical calculations for phthalazine derivatives as corrosion inhibitors of mild steel in 1M HCl, Corros. Sci. 56 (2012) 176–183.
[20] A.K. Singh, M.A. Quraishi, Effect of 2,2′ benzothiazolyl disulfide on the corrosion of mild steel in acid media, Corros. Sci. 51 (2009) 2752–2760.
[21] A. Suhasaria, M. Murmu, S. Satpati, P. Banerjee, D. Sukul, Bis-benzothiazoles as efficient corrosion inhibitors for mild steel in aqueous HCl: molecular structure-reactivity correlation study, J. Mol. Liq. 313 (2020) 113537.
[22] B. Chugh, A.K. Singh, D. Poddar, S. Thakur, B. Pani, P. Jain, Relation of degree of substitution and metal protecting ability of cinnamaldehyde modified chitosan, Carbohydr. Polym. 234 (2020) 115945.
[23] A.K. Singh, B. Chugh, S.K. Saha, P. Banerjee, E.E. Ebenso, S. Thakur, B. Pani, Evaluation of anti-corrosion performance of an expired semi synthetic antibiotic cefdinir for mild steel in 1 M HCl medium: an experimental and theoretical study, Results Phys. 14 (2019) 102383.
[24] J. Haque, V. Srivastava, M.A. Quraishi, D.S. Chauhan, H. Lgaz, I.M. Chung, Polar group substituted imidazolium zwitterions as eco-friendly corrosion inhibitors for mild steel in acid solution, Corros. Sci. 172 (2020) 108665.
[25] V.P. Singh, S. Singh, N′-[1-(2-Aminophenyl) ethylidene] benzohydrazide, Acta Cryst. E. 66 (2010) o1172.
[26] A.K. Singh, S. Mohapatra, B. Pani, Corrosion inhibition effect of *Aloe Vera* gel: gravimetric and electrochemical study, J. Ind. Eng. Chem. 33 (2016) 288–297.
[27] A.K. Singh, Inhibition of mild steel corrosion in hydrochloric acid solution by 3-(4-((Z)-Indolin-3-ylideneamino)phenylimino)indolin-2-one, Ind. Eng. Chem. Res. 51 (2012) 3215–3223.
[28] A.K. Singh, P. Singh, Adsorption behaviour of o-hydroxy acetophenone benzoyl hydrazone on mild steel/hydrochloric acid interface, J. Ind. Eng. Chem. 21 (2015) 552–560.
[29] A.D. Becke, A new mixing of Hartree–Fock and local density-functional theories, J. Chem. Phys. 98 (1993) 1372–1377.
[30] C. Lee, W. Yang, R.G. Parr, Development of the Colle-Salvetti correlation-energy formula into a functional of the electron density, Phys. Rev. B 37 (1988) 785–789.
[31] M.J. Frisch, G.W. Trucks, H.B. Schlegel, G.E. Scuseria, M.A. Robb, J.R. Cheeseman, G. Scalmani, V. Barone, B. Mennucci, G.A. Petersson, H. Nakatsuji, M. Caricato, X. Li, H.P. Hratchian, A.F. Izmaylov, J. Bloino, G. Zheng, J.L. Sonnenberg, M. Hada, M. Ehara, K. Toyota, R. Fukuda, J. Hasegawa, M. Ishida, T. Nakajima, Y. Honda, O. Kitao, H. Nakai, T. Vreven, J.A. Montgomery Jr., J.E. Peralta, F. Ogliaro, M. Bearpark, J.J. Heyd, E. Brothers, K.N. Kudin, V.N. Staroverov, T. Keith, R. Kobayashi, J. Normand, K. Raghavachari, A. Rendell, J.C. Burant, S.S. Iyengar, J. Tomasi, M. Cossi, N. Rega, J.M. Millam, M. Klene, J.E. Knox, J.B. Cross, V. Bakken, C. Adamo, J. Jaramillo, R. Gomperts, R.E. Stratmann, O. Yazyev, A.J. Austin, R. Cammi, C. Pomelli, J.W. Ochterski, R.L. Martin, K. Morokuma, V.G. Zakrzewski, G.A. Voth, P. Salvador, J.J. Dannenberg, S. Dapprich, A.D. Daniels, O. Farkas, J.B. Foresman, J.V. Ortiz, J. Cioslowski, D.J. Fox, Gaussian 09 D.01, Gaussian, Inc, Wallingford CT, 2013.
[32] A.V. Marenich, C.J. Cramer, D.G. Truhlar, Universal solvation model based on solute Electron density and on a continuum model of the solvent defined by the bulk dielectric constant and atomic surface tensions, J. Phys. Chem. B 113 (2009) 6378–6396.
[33] F. Weinhold, C.R. Landis, E.D. Glendening, What is NBO analysis and how is it useful? Int. Rev. Phys. Chem. 35 (2016) 399–440.
[34] A.E. Reed, L.A. Curtiss, F. Weinhold, Intermolecular interactions from a natural bond orbital, donor-acceptor viewpoint, Chem. Rev. 88 (1988) 899–926.
[35] T. Koopmans, Über die Zuordnung von Wellenfunktionen und Eigenwerten zu den einzelnen Elektronen eines Atoms, Physica. 1 (1934) 104–113.
[36] R.G. Parr, L.V. Szentpaly, S. Liu, Electrophilicity index, J. Am. Chem. Soc. 121 (1999) 1922–1924.
[37] R.G. Parr, R.G. Pearson, Absolute hardness: companion parameter to absolute electronegativity, J. Am. Chem. Soc. 105 (1983) 7512–7516.
[38] N. Islam, S. Kaya (Eds.), Conceptual Density Functional Theory and its Application in the Chemical Domain, CRC Press, 2018.
[39] S. Kaya, C. Kaya, A new equation based on ionization energies and electron affinities of atoms for calculating of group electronegativity, Comput. Theor. Chem. 1052 (2015) 42–46.
[40] P.K. Chattaraj, S. Duley, L.R. Domingo, Understanding local electrophilicity/nucleophilicity activation through a single reactivity difference index, Org. Biomol. Chem. 10 (2012) 2855–2861.
[41] J.L. Gazquez, A. Cedillo, A. Vela, Electrodonating and electroaccepting powers, J. Phys. Chem. A 111 (2007) 1966–1970.
[42] A. Pandey, B. Singh, C. Verma, M.A. Quraishi, Synthesis, characterization and corrosion inhibition potential of two novel Schiff bases on mild steel in acidic medium, RSC Adv. 7 (2017) 47148–47163.
[43] A.K. Singh, B. Chugh, S. Thakur, B. Pani, H. Lgaz, I.M. Chung, S. Pal, R. Prakash, Green approach of synthesis of thiazolyl imines and their impeding behavior against corrosion of mild steel in acid medium, Colloids Surf. A Physicochem. Eng. Asp. 599 (2020) 124824.
[44] M. Srivastava, P. Tiwari, S.K. Srivastava, A. Kumar, G. Ji, R. Prakash, Low cost aqueous extract of *Pisum sativum* peels for inhibition of mild steel corrosion, J. Mol. Liq. 254 (2018) 357–368.
[45] M. Rbaa, M. Fardioui, C. Verma, A.S. Abousalem, M. Galai, E.E. Ebenso, T. Guedira, B. Lakhrissi, I. Warad, A. Zarrouk, 8-Hydroxyquinoline based chitosan derived carbohydrate polymer as biodegradable and sustainable acid corrosion inhibitor for mild steel: Experimental and computational analyses, Int. J. Biol. Macromol. 155 (2020) 645–655.
[46] A.K. Singh, M.A. Quraishi, Investigation of the effect of disulfiram on corrosion of mild steel in hydrochloric acid solution, Corros. Sci. 53 (2011) 1288–1297.
[47] A.K. Singh, M.A. Quraishi, Inhibitive effect of diethylcarbamazine on the corrosion of mild steel in hydrochloric acid, Corros. Sci. 52 (2010) 1529–1535.
[48] E. Berdimurodov, A. Kholikov, K. Akbarov, G. Xu, A.M. Abdullah, M. Hosseini, New anti-corrosion inhibitor (3ar,6ar)-3a,6a-di-p-tolyltetrahydroimidazo[4,5-d]imidazole-2,5(1*h*,3h)-dithione for carbon steel in 1 M HCl medium: gravimetric, electrochemical, surface and quantum chemical analyses, Arab. J. Chem. 13 (2020) 7504–7523.
[49] A.K. Singh, M.A. Quraishi, Effect of cefazolin on the corrosion of mild steel in HCl solution, Corros. Sci. 52 (2010) 152–160.
[50] E.A. Abd El-Wahab, A.H. Marei, O.R. Khalifa, H.A. Mohamed, Corrosion behavior of aluminum electrode in absence and in presence of sodium chloride at different pH solutions using Toludine as inhibitor, J. Am. Sci. 6 (2010) 476–486.
[51] B. Chugh, A.K. Singh, A. Chaouiki, R. Salghi, S. Thakur, B. Pani, A comprehensive study about anti-corrosion behaviour of pyrazine carbohydrazide: gravimetric, electrochemical, surface and theoretical study, J. Mol. Liq. 299 (2020) 112160.
[52] G. Ji, S. Anjum, S. Sundaram, R. Prakash, Musa paradisica peel extract as green corrosion inhibitor for mild steel in HCl solution, Corros. Sci. 90 (2015) 107–117.
[53] A.K. Singh, A.K. Pandey, P. Banerjee, S.K. Saha, B. Chugh, S. Thakur, B. Pani, P. Chaubey, G. Singh, Eco-friendly disposal of expired anti-tuberculosis drug isoniazid and its role in the protection of metal, J. Environ. Chem. Eng. 7 (2019) 102971.
[54] B. Chugh, A.K. Singh, S. Thakur, B. Pani, A.K. Pandey, H. Lgaz, I.M. Chung, E.E. Ebenso, An exploration about the interaction of mild steel with hydrochloric acid in the presence of N-(benzo[d] Thiazole-2-yl)-1-Phenylethan-1-imines, J. Phys. Chem. C 123 (2019) 22897–22917.
[55] A.F.S.A. Rahiman, S. Sethumanickam, Corrosion inhibition, adsorption and thermodynamic properties of poly(vinyl alcohol-cysteine) in molar HCl, Arab. J. Chem. 10 (2017) S3358–S3366.
[56] A. Hamdy, N.Sh. El-Gendy, Thermodynamic, adsorption and electrochemical studies for corrosion inhibition of carbon steel by henna extract in acid medium, Egypt. J. Pet. 22 (2013) 17–25.
[57] A.K. Singh, S. Thakur, B. Pani, Eno E. Ebenso, M.A. Quraishi, A.K. Pandey, 2-Hydroxy-N′-((Thiophene-2-yl)methylene) benzohydrazide: Ultrasound-assisted synthesis and corrosion inhibition study, ACS Omega 3 (2018) 4695–4705.
[58] A.K. Singh, M.A. Quraishi, The effect of some bis-thiadiazoles derivatives on the corrosion of mild steel in hydrochloric acid, Corros. Sci. 52 (2010) 1373–1385.
[59] A.R. Hoseizadeh, I. Danaee, M.H. Maddahy, Adsorption and corrosion inhibitive properties of 2-Mercaptobenzothiazole on AISI steel 4130 alloy in hydrochloric acid solution, Kovove Mater. 52 (2014) 35–45.
[60] V. Branzoi, F. Branzoi, M. Baibarac, The inhibition of the corrosion of Armco … of N-alkyl quaternary ammonium salts, Mater. Chem. Phys. 65 (2000) 288–297.
[61] A.K. Singh, S. Thakur, B. Pani, G. Singh, Green synthesis and corrosion inhibition study of 2-amino-N′-((thiophen-2-yl)methylene)benzohydrazide, New J. Chem. 42 (2018) 2113–2124.
[62] W. Zhang, H.-J. Li, Y. Wang, Y. Liu, Q.-Z. Gu, Y.-C. Wu, Gravimetric, electrochemical and surface studies on the anticorrosive properties of 1-(2-pyridyl)-2-thiourea and 2- (imidazol-2-yl)-pyridine for mild steel in hydrochloric acid, New J. Chem. 42 (2018) 12649–12665.
[63] A.K. Singh, B. Chugh, S. Thakur, B. Pani, H. Lgaz, I.M. Chung, P. Chaubey, A.K. Pandey, J. Singh, Solvent-free microwave assisted synthesis and corrosion inhibition study of a series of hydrazones derived from thiophene derivatives: experimental, surface and theoretical study, J. Mol. Liq. 283 (2019) 788–803.
[64] S. Cao, D. Liu, P. Zhang, L. Yang, P. Yang, H. Lu, J. Gui, Green Brönsted acid ionic liquids as novel corrosion inhibitors for carbon steel in acidic medium, Sci. Rep. 7 (2017) 8773.
[65] A. Saeed, N. Arshad, A.K. Singh, B. Chugh, M. Akram, F. Perveen, I. Rasheed, F. Altaf, P.A. Channar, Experimental, theoretical, and surface study for corrosion inhibition of mild steel in 1 M HCl by using synthetic anti-biotic derivatives, Ionics. 25 (2019) 5057–5075.
[66] M. Tourabi, K. Nohair, M. Traisnel, C. Jama, F. Bentiss, Electrochemical and XPS studies of the corrosion inhibition of carbon steel in hydrochloric acid pickling solutions, Corros. Sci. 75 (2013) 123–133.
[67] A.S. Fouda, M. Eissa, G.Y. Elewady, W.T. El, Corrosion inhibition of low carbon steel in 1 M HCl solution using Pulicaria Undulata plant extract, Int. J. Electrochem. Sci. 12 (2017) 9212–9230.
[68] Z. Cao, Y. Tang, H. Cang, J. Xu, G. Lu, W. Jing, Novel Benzimidazole derivatives as corrosion inhibitors of mild steel in the acidic media, Corros. Sci. 83 (2014) 292–298.
[69] B. Chugh, A.K. Singh, S. Thakur, B. Pani, H. Lgaz, I.M. Chung, R. Jha, E.E. Ebenso, Comparative investigation of corrosion-mitigating behavior of Thiadiazole-derived Bis-Schiff bases for mild steel in acid medium: experimental, theoretical, and surface study, ACS Omega. 5 (2020) 13503–13520.

[70] P.K. Chattaraj, H. Lee, R.G. Parr, HSAB principle, J. Am. Chemical Society 113 (1991) 1855–1856.
[71] S. Kaya, C. Kaya, A new equation for calculation of chemical hardness of groups and molecules, Mol. Phys. 113 (2015) 1311–1319.
[72] S. Kaya, C. Kaya, A simple method for the calculation of lattice energies of inorganic ionic crystals based on the chemical hardness, Inorg. Chem. 54 (2015) 8207–8213.
[73] S. Pan, M. Solà, P.K. Chattaraj, On the validity of the maximum hardness principle and the minimum electrophilicity principle during chemical reactions, J. Phys. Chem. A 117 (2013) 1843–1852.
[74] S. Kaya, C. Kaya, N. Islam, Maximum hardness and minimum polarizability principles through lattice energies of ionic compounds, Physica. B. Condens. Matter. 485 (2016) 60–66.